

See discussions, stats, and author profiles for this publication at: <https://www.researchgate.net/publication/329387794>

Disentangling Adversarial Robustness and Generalization

Preprint · December 2018

CITATIONS

0

READS

94

3 authors, including:



[David Stutz](#)

Max Planck Institute for Informatics

14 PUBLICATIONS 545 CITATIONS

SEE PROFILE

Disentangling Adversarial Robustness and Generalization

David Stutz¹ Matthias Hein² Bernt Schiele¹

¹Max Planck Institute for Informatics, ²University of Tübingen

¹{david.stutz,schiele}@mpi-inf.mpg.de, ²matthias.hein@uni-tuebingen.de

Abstract

Obtaining deep networks that are robust against adversarial examples and generalize well is an open problem. A recent hypothesis [97, 90] even states ~~that~~ ^{true} both robust and accurate models are impossible, i.e., adversarial robustness and generalization are conflicting goals. In an effort to clarify the relationship between robustness and generalization, we assume an underlying, low-dimensional data manifold and show that: 1. regular adversarial examples leave the manifold; 2. adversarial examples constrained to the manifold, i.e., on-manifold adversarial examples, exist; 3. on-manifold adversarial examples are generalization errors, and on-manifold adversarial training boosts generalization; 4. and regular robustness is independent of generalization. These assumptions imply that both robust and accurate models are possible. However, different models (architectures, training strategies etc.) can exhibit different robustness and generalization characteristics. To confirm our claims, we present extensive experiments on synthetic data (with access to the true manifold) as well as on EMNIST [19], Fashion-MNIST [101] and CelebA [58].

1. Introduction

Adversarial robustness describes a deep network’s ability to defend against adversarial examples [92], imperceptibly perturbed images causing mis-classification. These adversarial attacks pose severe security threats, as demonstrated against Clarifai.com [56, 8] or Google Cloud Vision [36]. Despite these serious risks, defenses against such attacks have been largely ineffective; only adversarial training, i.e., training on adversarial examples [62, 30], has been shown to work well in practice [6, 5] – at the cost of computational overhead and reduced accuracy. Overall, the problem of adversarial robustness is left open and poorly understood – even for simple datasets such as EMNIST [19] and Fashion-MNIST [101].

The phenomenon of adversarial examples itself, i.e., their mere existence, has also received considerable attention. Recently, early explanations, e.g., attributing adver-

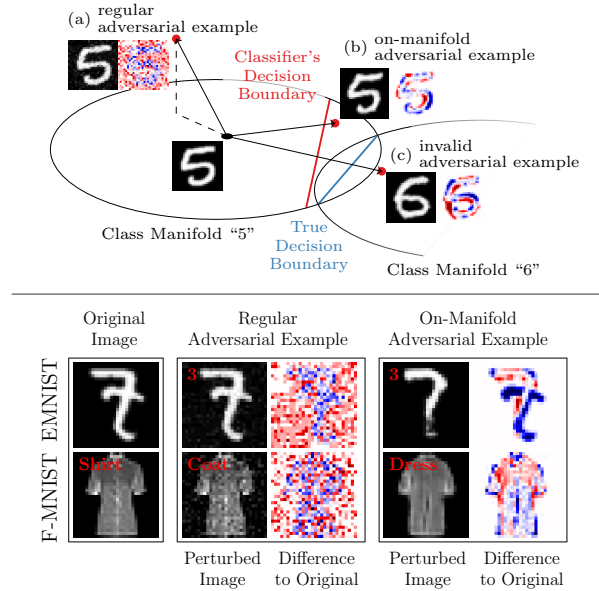


Figure 1: Adversarial examples, and their (normalized) difference to the original image, in the context of the underlying manifold, e.g., class manifolds “5” and “6” on EMNIST [19], allow to study their relation to generalization. Regular adversarial examples are not constrained to the manifold, cf. (a), and often result in (seemingly) random noise patterns; in fact, we show that they leave the manifold. However, adversarial examples on the manifold can be found as well, cf. (b), resulting in meaningful manipulations of the image content; however, care needs to be taken that the actual, true label wrt. the manifold does not change, cf. (c).

arial examples to “rare pockets” of the classification surface [92] or linearities in deep networks [30], have been superseded by the manifold assumption [27, 94]: adversarial examples are assumed to leave the underlying, low-dimensional but usually unknown data manifold. Yet, on a simplistic toy dataset, Gilmer et al. [27] also found adversarial examples on the manifold, as also tried on real datasets [88, 11, 106], rendering the manifold assumption questionable. Still, the manifold assumption fostered research on novel defenses [38, 72, 80].

Beyond the existence of adversarial examples, their relation to generalization is an important open problem. Re-

cently, it has been argued [97, 90] that there exists an inherent trade-off, i.e., robust and accurate models seem impossible. While Tsipras et al. [97] provide a theoretical argument on a toy dataset, Su et al. [90] evaluate the robustness of different models on ImageNet [78]. However, these findings have to be questioned given the results in [27, 76] showing the opposite, i.e., better generalization helps robustness. In light of this controversy, in this study, we adopt the hypothesis by Tsipras et al.:

*Models **cannot** be both robust and accurate.*

In order to address this hypothesis, and in contrast to [97, 91, 76], we consider adversarial robustness in the context of the underlying manifold. In particular, to break the hypothesis down, we explicitly ask whether adversarial examples leave, or stay on, the manifold. On EMNIST, for example, considering the class manifolds for “5” and “6”, as illustrated in Fig. 1, adversarial examples are not guaranteed to lie on the manifold, cf. Fig. 1 (a). Adversarial examples can, however, also be constrained to the manifold, cf. Fig. 1 (b); in this case, it is important to ensure that the adversarial examples do not actually change their label, i.e., are more likely to be a “6” than a “5”, as in Fig. 1 (c). For clarity, we refer to unconstrained adversarial examples, as illustrated in Fig. 1 (a), as *regular adversarial examples*; in contrast to adversarial examples constrained to the manifold, so-called *on-manifold adversarial examples*.

Contributions: Based on this distinction between regular robustness, i.e., against regular, unconstrained adversarial examples, and on-manifold robustness, i.e., against adversarial examples constrained to the manifold, we show:

1. regular adversarial examples leave the manifold;
2. adversarial examples constrained to the manifold, i.e., **on-manifold adversarial examples**, exist and can be computed using an approximation of the manifold;
3. **on-manifold robustness** is essentially generalization;
4. regular robustness is independent of generalization.

We conclude that **both robust and accurate models are possible**; specifically, for any arbitrary but fixed model, better generalization does not worsen robustness. Additionally, we propose **on-manifold adversarial training** to boost generalization in settings where the manifold is known, can be approximated, or invariances of the data are known. We present experimental results on a novel MNIST-like, synthetic dataset with known manifold, as well as on EMNIST [19], Fashion-MNIST [101] and CelebA [58]. We will make our code, data and results publicly available.

2. Related Work

We briefly discuss related work; however, we refer the reader to [104, 1, 9] for more comprehensive surveys.

Attacks: Adversarial examples for deep networks were first

reported in [92]; the problem of adversarial machine learning, however, has already been studied earlier [9]. Adversarial attacks on deep networks range from white-box attacks [92, 30, 48, 71, 66, 61, 14, 77, 20, 59], with full access to the model (weights, gradients etc.), to black-box attacks [17, 10, 91, 37, 79, 67], with limited access to model queries. White-box attacks based on first-order optimization, e.g., [61, 14], are considered state-of-the-art. Due to their transferability [57, 103, 70], these attacks can also be used in a black-box setting (e.g. using model stealing [85, 70, 96, 98, 69, 42]) and have, thus, become standard for evaluation. Recently, generative models have also been utilized to craft – or learn – more natural adversarial examples [88, 11, 107, 80]. Finally, adversarial examples have been applied to a wide variety of tasks, also beyond computer vision, e.g., [26, 18, 93, 47, 35, 54, 3, 16].

Defenses: Proposed defenses include detection and rejection methods [31, 25, 53, 60, 4, 63], pre-processing, quantization and dimensionality reduction methods [12, 73, 7], manifold-projection methods [38, 72, 80, 84], methods based on stochasticity/regularization or adapted architectures [105, 7, 68, 86, 33, 41, 75, 43, 49, 102], ensemble methods [55, 89, 32, 95], as well as adversarial training [105, 65, 34, 81, 87, 52, 61]; however, many defenses have been shown to be ineffective [13, 15, 5, 6]. In [6], only adversarial training, e.g., the work by Madry et al. [61], has been shown to be effective – although many recent defenses have not been studied extensively. Manifold-based methods, in particular, have received some attention lately: in [38, 72], generative adversarial networks [29] are used to project an adversarial example back to the learned manifold. Similarly, in [80], variational auto-encoders [46] are used to perform robust classification.

Generalization: Research also includes independent benchmarks of attacks and defenses [13, 15, 5, 6, 83], their properties [57, 82], as well as theoretical questions [33, 41, 22, 94, 27, 86, 97, 99]. Among others, the existence of adversarial examples [92, 30, 94] raises many questions. While Szegedy et al. [92] originally thought of adversarial examples as “extremely” rare negatives and Goodfellow et al. [30] attributed adversarial examples to the linearity in deep networks, others argued against these assumptions [27, 94]. Instead, a widely accepted theory is the manifold assumption; adversarial examples are assumed to leave the data manifold [27, 94, 38, 72, 80].

This paper is particularly related to work on the connection of adversarial examples to generalization [97, 90, 27, 76]. Tsipras et al. [97] and Su et al. [90] argue that there exists an inherent trade-off between robustness and generalization. However, the theoretical argument in [97] is questionable as adversarial examples are allowed to change their actual, true label wrt. the data distribution, as illustrated Fig. 1 (c). The experimental results obtained in [90, 76]

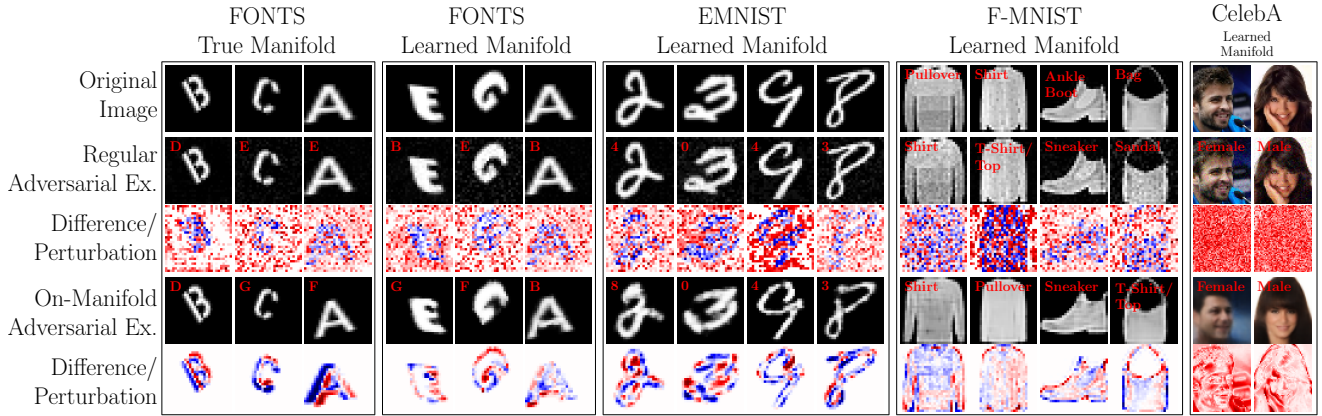


Figure 2: Regular and on-manifold adversarial examples on our synthetic dataset, FONTS, consisting of randomly transformed characters “A” to “J”, EMNIST [19], F-MNIST [101] and CelebA [58]. On FONTS, the manifold is known by construction; in the other cases, the class manifolds have been approximated using VAE-GANs [50, 74]. The difference (normalized; or their magnitude on CelebA) to the original test image reveals the (seemingly) random noise patterns of regular adversarial examples in contrast to reasonable concept changes of on-manifold adversarial examples.

stem from comparing different architectures and training strategies; in contrast, we consider robustness and generalization for any arbitrary but fixed model. On a synthetic toy dataset, Gilmer et al. [27] show that on-manifold adversarial examples exist. We further show that on-manifold adversarial examples also exist on real datasets with unknown manifold, similar to [107]. In contrast to [107], however, we utilize a gradient-based attack on the manifold. Finally, our work is also related to [24] and [65, 64] where variants of adversarial training are used to boost (semi-)supervised learning. While, e.g., Fawzi et al. [24], apply adversarial training to image transformations, we further perform adversarial training on adversarial examples constrained to the true, or approximated, manifold. Overall, despite the growing interest in the relationship of robustness and generalization, it has not been resolved yet.

3. Disentangling Adversarial Robustness and Generalization

To clarify the relationship between adversarial robustness and generalization, we explicitly distinguish between regular and on-manifold adversarial examples, as illustrated in Fig. 1. Then, the hypothesis [97, 90] that robustness and generalization are at odds is challenged in four arguments: regular adversarial examples leave the manifold; adversarial examples constrained to the manifold exist; and robustness against on-manifold adversarial examples is essentially generalization, while robustness against regular adversarial examples is independent of generalization. Altogether, our results imply that adversarial robustness and generalization are not opposing objectives.

3.1. Experimental Setup

Datasets: We use EMNIST [19], F(ashion)-MNIST [101] and CelebA [58] for our experiments (240k/40k, 60k/10k and 182k/20k training/test images); CelebA has been resized to 56×48 and we classify “Male” vs. “Female”. Our synthetic dataset, FONTS, consists of letters “A” to “J” of 1000 Google Fonts randomly transformed (uniformly over translation, shear, scale, rotation in $[-0.2, 0.2]$, $[-0.5, 0.5]$, $[0.75, 1.15]$, $[-\pi/2, \pi/2]$) using a spatial transformer network [40] such that the generation process is completely differentiable. The latent variables correspond to the transformation parameters, font and class. We generated 960k/40k (balanced) training/test images of size 28×28 .

We consider classifiers with three (four on CelebA) convolutional layers (4×4 kernels; stride 2; 16, 32, 64 channels), each followed by ReLU activations and batch normalization [39], and two fully connected layers. The networks are trained using ADAM [45], with learning rate 0.01 (decayed by 0.95 per epoch), weight decay 0.0001 and batch size 100, for 20 epochs. Most importantly, to control their generalization performance, we use N training images, with N between 250 and 40k; for each N , we train 5 models with random weight initialization [28] and report averages.

We learn class-specific VAE-GANs, similar to [50, 74], to approximate the underlying manifold; we refer to the supplementary material for details.

Attack: Given an image-label pair (x, y) from an unknown data distribution p and a classifier f , an adversarial example is a perturbed image $\tilde{x} = x + \delta$ which is mis-classified by the model, i.e., $f(\tilde{x}) \neq y$. While our results can be confirmed using other attacks and norms (see the supplementary material for [14] and transfer attacks), for clarity, we concentrate on the L_∞ white-box attack by Madry et al.

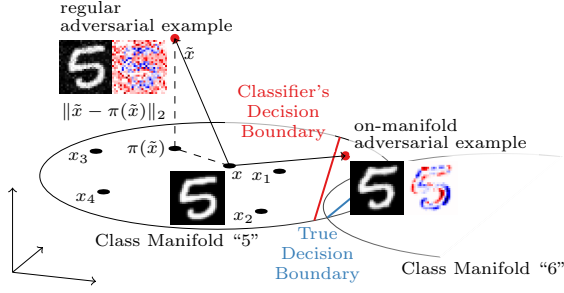


Figure 3: The distance of a regular adversarial example \tilde{x} to the manifold, as approximated using nearest neighbors, is computed as the distance to its orthogonal projection $\pi(\tilde{x})$ onto the manifold: $\|\tilde{x} - \pi(\tilde{x})\|_2$. Large distance indicates that the adversarial example is likely to have left the manifold, i.e., is off-manifold.

[62] that directly maximizes the training loss,

$$\max_{\delta} \mathcal{L}(f(x + \delta), y) \quad \text{s.t.} \quad \|\delta\|_{\infty} \leq \epsilon, \tilde{x}_i \in [0, 1], \quad (1)$$

using projected gradient descent; where \mathcal{L} is the cross-entropy loss. The ϵ -constraint is meant to ensure perceptual similarity. We run 40 iterations of ADAM [45] with learning rate 0.005 and consider 5 restarts, (distance and direction) uniformly sampled in the ϵ -ball for $\epsilon = 0.3$. Optimization is stopped as soon as the predicted label changes, i.e., $f(\tilde{x}) \neq y$. We attack 1000 test images.

Adversarial Training: An established defense is adversarial training, i.e., training on adversarial examples crafted during training [105, 65, 34, 81, 87, 52, 62]. Madry et al. [62] consider the min-max problem

$$\min \sum_{n=1}^N \max_{\|\delta\|_{\infty} \leq \epsilon} \mathcal{L}(f(x_n + \delta; w), y_n) \quad (2)$$

where w are the classifier’s weights and x_n the training images. As shown in the supplementary material, we considered different variants [92, 30, 62]; in the paper, however, we follow common practice and train on 50% clean images and 50% adversarial examples [92]. For $\epsilon = 0.3$, the attack (for the inner optimization problem) is run for full 40 iterations, i.e., is not stopped at the first adversarial example found. Robustness of the obtained network is measured by computing the attack **success rate**, i.e., the fraction of successful attacks on correctly classified test images, as, e.g., in [14], for a fixed ϵ ; lower success rate indicates higher robustness of the network.

3.2. Adversarial Examples Leave the Manifold

The idea of adversarial examples leaving the manifold can be illustrated on EMNIST where particular background pixels are known to be constant, see Fig. 2. If an adversarial example \tilde{x} manipulates these pixels, it has zero probability under the data distribution and its distance to the manifold, in terms of the distance to its projection $\pi(\tilde{x})$ onto

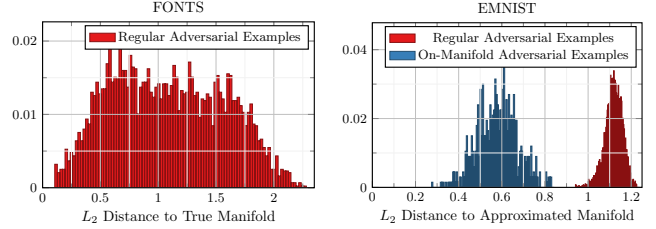


Figure 4: Distance of adversarial examples to the true, on FONTS (left), or approximated, on EMNIST (right), manifold. We show normalized histograms of the L_2 distance of adversarial examples to their projections onto the manifold (4377/3837 regular adversarial examples on FONTS/EMNIST; 667 on-manifold adversarial examples on EMNIST). Regular adversarial examples exhibit a significant distance to the manifold; on EMNIST, clearly distinguishable from on-manifold adversarial examples.

the manifold, should be non-zero. On FONTS, with known generative process in the form of a decoder dec mapping latent variables z to images x , the projection is obtained iteratively: $\pi(\tilde{x}) = \text{dec}(\tilde{z})$ with $\tilde{z} = \arg\min_z \|\text{dec}(z) - \tilde{x}\|_2$ and z constrained to valid transformations (font and class, known from the test image x , stay constant). On EMNIST, as illustrated in Fig. 3, the manifold is approximated using 50 nearest neighbors; the projection $\pi(\tilde{x})$ onto the subspace spanned by the x -centered nearest neighbors is computed through least squares. On both FONTS and EMNIST, the distance $\|\tilde{x} - \pi(\tilde{x})\|_2$ is considered to assess whether the adversarial example \tilde{x} actually left the manifold.

On FONTS, Fig. 4 (left) shows that regular adversarial examples clearly exhibit non-zero distance to the manifold. In fact, the projections of these adversarial examples to the manifold are almost always the original test images; as a result, the distance to the manifold is essentially the norm of the corresponding perturbation: $\|\tilde{x} - \pi(\tilde{x})\|_2 \approx \|\tilde{x} - x\|_2 = \|\delta\|_2$. This suggests that the adversarial examples leave the manifold in an almost orthogonal direction. On EMNIST, in Fig. 4 (right), these results can be confirmed in spite of the crude local approximation of the manifold. Again, regular adversarial examples seem to leave the manifold almost orthogonally, i.e., their distance to the manifold coincides with the norm of the corresponding perturbations. These results can be confirmed on F-MNIST, see the supplementary material, and show that regular adversarial examples essentially *are* off-manifold adversarial examples; this finding is intuitive as for well-trained classifiers, leaving the manifold should be the “easiest” way to fool it.

3.3. On-Manifold Adversarial Examples

Given that regular adversarial examples leave the manifold, we intend to explicitly compute on-manifold adversarial examples. To this end, we assume our data distribution $p(x, y)$ to be conditional on the latent variables

z , i.e., $p(x, y|z)$, corresponding to the underlying, low-dimensional manifold. On this manifold, however, there is no notion of “perceptual similarity” in order to ensure label invariance. In terms of Fig. 1, ensuring label invariance requires to distinguish valid on-manifold adversarial examples, Fig. 1 (b), from invalid ones that change the actual, true label, Fig. 1 (c):

Definition 1 (On-Manifold Adversarial Example). Given the data distribution p , an on-manifold adversarial example for x with label y is a perturbed version \tilde{x} such that $f(\tilde{x}) \neq y$ but $p(y|\tilde{x}) > p(y'|\tilde{x}) \forall y' \neq y$.

Note that the posteriors $p(y|\tilde{x})$ correspond to the true, unknown data distribution; any on-manifold adversarial example \tilde{x} violating Def. 1 changed its actual, true label.

In practice, we assume access to an encoder and decoder modeling the (class-conditional) distributions $p(z|x, y)$ and $p(x|z, y)$ – in our case, achieved using VAE-GANs [50, 74]. Then, given the encoder and as illustrated in Fig. 5, we obtain the latent code $z = \text{enc}(x)$ and compute the perturbation ζ by maximizing:

$$\max_{\zeta} \mathcal{L}(f(\text{dec}(z + \zeta)), y) \quad \text{s.t.} \quad \|\zeta\|_{\infty} \leq \eta. \quad (3)$$

The image-constraint, i.e., $\tilde{x}_i \in [0, 1]$ for $\tilde{x} = \text{dec}(z + \zeta)$, is usually enforced by the decoder; the η -constraint can, again, be enforced by projection; and we can additionally enforce a constraint on $z + \zeta$, e.g., corresponding to a prior on z . Label invariance, as in Def. 1, is ensured by explicitly considering only class-specific encoders and decoders, i.e., the data distribution is approximated per class¹. We use $\eta = 0.3$ and the same optimization procedure as for Eq. (1); on approximated manifolds, the perturbation $z + \zeta$ is additionally constrained to $[-2, 2]$ ¹⁰, corresponding to a truncated normal prior from the class-specific VAE-GANs; we attack 2500 test images.

On-manifold adversarial examples obtained through Eq. (3) are similar to those crafted in [27], [80], [6] or [107]. However, in contrast to [27, 80, 6], we directly compute the perturbation ζ on the manifold instead of computing the perturbation δ in the image space and subsequently projecting $x + \delta$ to the manifold. Also note that enforcing any similarity constraint through a norm on the manifold is significantly more meaningful compared to using a norm on the image space, as becomes apparent when comparing the obtained on-manifold adversarial examples in Fig. 2 to their regular counterparts. Compared to [107], we find on-manifold adversarial examples using a gradient-based approach instead of randomly sampling the latent space.

Fig. 2 shows on-manifold adversarial examples for all datasets, which we found significantly harder to obtain

¹In the supplementary material we also consider the case of class-agnostic VAE-GAN manifolds, leading to similar results; then, label invariance needs to be ensured using smaller η .

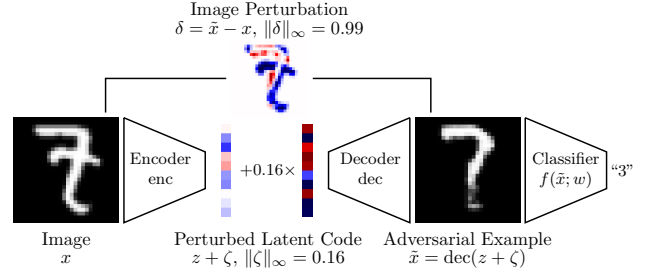


Figure 5: **On-manifold adversarial examples can be computed using learned, class-specific VAE-GANs [50, 74].** Using the obtained encoder and decoder, the perturbation ζ is obtained via Eq. (3) and added to $z = \text{enc}(x)$ yielding the adversarial example $\tilde{x} = \text{dec}(z + \zeta)$. In image space, the difference $\delta = \tilde{x} - x$ illustrates how the content of the image changes.

compared to their regular counterparts. On FONTS, using the true, known class manifolds, on-manifold adversarial examples clearly correspond to transformations of the original test image – reflecting the true latent space. For the learned class manifolds, the perturbations are less pronounced, often manipulating boldness or details of the characters. Due to the approximate nature of the learned VAE-GANs, these adversarial examples are strictly speaking not always part of the true manifold – as can be seen for the irregular “A” (Fig. 2, 6th column). On EMNIST and FMNIST, on-manifold adversarial examples represent meaningful manipulations, such as removing the tail of a hand-drawn “8” (Fig. 2, 10th column) or removing the collar of a pullover (Fig. 2, 11th column), in contrast to the random noise patterns of regular adversarial examples. However, these usually incur a smaller change in the images space; which also explains why regular, unconstrained adversarial examples almost always leave the manifold. Still, on-manifold adversarial examples are perceptually close to the original images. On CelebA, the quality of on-manifold adversarial examples is clearly limited by the approximation quality of our VAE-GANs. Finally, Fig. 4 (right) shows that on-manifold adversarial examples are closer to the manifold than regular adversarial examples – in spite of the crude approximation of the manifold on EMNIST.

3.4. On-Manifold Robustness is Essentially Generalization

We argue that on-manifold robustness is nothing different than generalization: as on-manifold adversarial examples have non-zero probability under the data distribution, they are merely generalization errors. This is shown in Fig. 6 (top left) where test error and on-manifold success rate on FONTS are shown. As expected, better generalization, i.e., using more training images N , also reduces on-manifold success rate. In order to make this relationship explicit, Fig. 6 (bottom) plots on-manifold success rate against

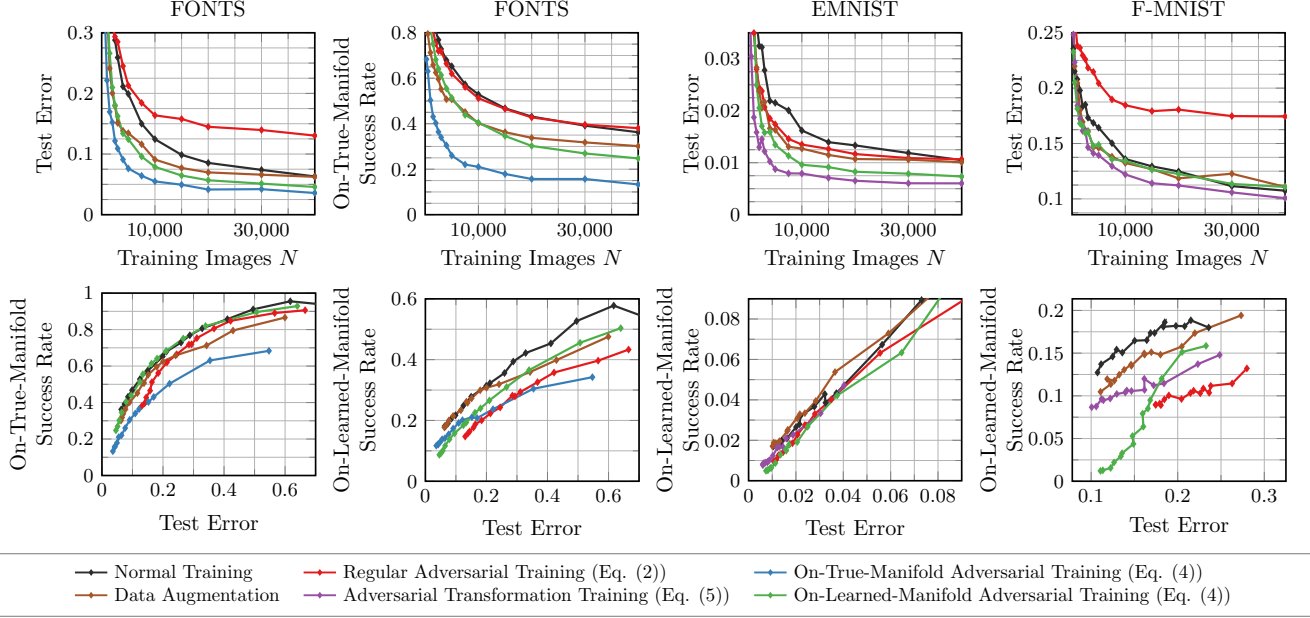


Figure 6: On-manifold robustness is strongly related to generalization, as shown on FONTS, EMNIST and F-MNIST considering on-manifold success rate and test error. Top: test error and on-manifold success rate in relation to the number of training images. As test error reduces, so does on-manifold success rate; furthermore, on-manifold adversarial training improves generalization. Bottom: on-manifold success rate plotted against test error reveals the strong relationship between on-manifold robustness and generalization.

test error. Then, especially for FONTS and EMNIST, the relationship of on-manifold robustness and generalization becomes apparent. On F-MNIST, the relationship is less pronounced because on-manifold adversarial examples, computed using our VAE-GANs, are not close enough to real generalization errors. However, even on F-MNIST, the experiments show a clear relationship between on-manifold robustness and generalization.

3.4.1 On-Manifold Adversarial Training Boosts Generalization

Given that generalization positively influences on-manifold robustness, we propose to adapt adversarial training to the on-manifold case **in order to boost generalization**:

$$\min_w \sum_{n=1}^N \max_{\|\zeta\|_\infty \leq \eta} \mathcal{L}(f(\text{dec}(z_n + \zeta); w), y_n). \quad (4)$$

with $z_n = \text{dec}(x_n)$ being the latent codes corresponding to training images x_n . Then, on-manifold adversarial training corresponds to robust optimization wrt. the true, or approximated, data distribution. For example, with perfect decoder on FONTS, the inner optimization problem finds “hard” images irrespective of their likelihood under the data distribution. For approximate dec, the benefit of on-manifold adversarial training depends on how well the true data distribution is matched, i.e., how realistic the obtained on-manifold adversarial examples are; in our case, this depends

on the quality of the learned VAE-GANs.

Instead of approximating the manifold using generative models, we can exploit known invariances of the data. Then, adversarial training can be applied to these invariances, assuming that they are part of the true manifold. In practice, this can, for example, be accomplished using adversarial deformations [2, 100, 21], i.e., adversarially crafted transformations of the image. For example, as on FONTS, we consider 6-degrees-of-freedom transformations corresponding to translation, shear, scaling and rotation:

$$\min_w \sum_{n=1}^N \max_{\|t\|_\infty \leq \eta, t \in \mathbb{R}^6} \mathcal{L}(f(T(x_n; t); w), y_n). \quad (5)$$

where $T(x; t)$ denotes the transformation of image x with parameters t and the η -constraint ensures similarity and label invariance. Again, the transformations can be applied using spatial transformer networks [40] such that T is differentiable; t can additionally be constrained to a reasonable space of transformations. We note that a similar approach has been used by Fawzi et al. [24] to boost generalization on, e.g., MNIST [51]. However, the approach was considered as an adversarial variant of data augmentation and not motivated through the lens of on-manifold robustness. We refer to Eq. (5) as adversarial transformation training and note that, on FONTS, this approach is equivalent to on-manifold adversarial training as the transformations coincide with the actual, true manifold by construction. We also include a data augmentation baseline, where the trans-

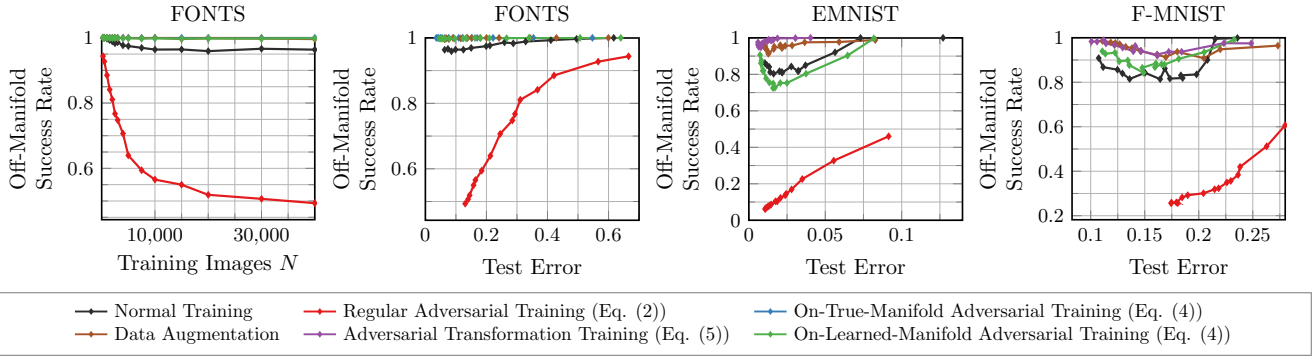


Figure 7: Regular robustness is not related to generalization, as demonstrated on FONTS, EMNIST and F-MNIST considering test error and (regular) success rate. On FONTS (left), success rate is not influenced by test error, except for adversarial training. Plotting success rate against test error highlights the independence of robustness and generalization; however, different training strategies exhibit different robustness-generalization characteristics.

formations t are applied randomly.

We demonstrate the effectiveness of on-manifold adversarial training in Fig. 6 (top). On FONTS, with access to the true manifold, on-manifold adversarial training is able to boost generalization significantly, especially for low N , i.e., few training images. Our VAE-GAN approximation on FONTS seems to be good enough to preserve the benefit of on-manifold adversarial training. On EMNIST and F-MNIST, the benefit reduces with the difficulty of approximating the manifold; this is the “cost” of imperfect approximation. While the benefit is still significant on EMNIST, it diminishes on F-MNIST. However, both on EMNIST and F-MNIST, identifying invariances and utilizing adversarial transformation training recovers the boost in generalization; especially in contrast to the random data augmentation baseline. Overall, on-manifold adversarial training is a promising tool for improving generalization and we expect its benefit to increase with better generative models.

3.5. Regular Robustness is Independent of Generalization

We argue that generalization, as measured *on* the manifold wrt. the data distribution, is mostly independent of regular robustness, i.e., against regular adversarial examples that leave the manifold. Specifically, in Fig. 7 (left) for FONTS, it can be observed that – except for adversarial training – the success rate is invariant to the test error. More intuitively, this can be seen when plotting the success rate against test error, cf. Fig. 7 (middle left); only for adversarial training there exists a clear relationship. Similar behavior can be observed on EMNIST and F-MNIST, see Fig. 7 (right). Here, it can also be seen that different training strategies (e.g., normal training vs. on-manifold adversarial training) exhibit different characteristics wrt. robustness and generalization. Overall, generalization does not influence regular robustness, which is in strong contrast to the positive relation of generalization to on-manifold ro-

bustness.

As mentioned in Section 1, these findings are in contrast to related work [97, 90] claiming that a trade-off between robustness and generalization exists. For example, Tsipras et al. [97] use a synthetic toy dataset to theoretically show that no model can be both robust and accurate (on this dataset). However, they allow the adversary to produce perturbations that change the actual, true label wrt. the data distribution, i.e., the considered adversarial examples are, strictly speaking, not adversarial examples according to Def. 1, see the supplementary material for details. Thus, it is unclear whether the suggested trade-off actually exists; our experiments seem to indicate the contrary. Similarly, Su et al. [90] experimentally show a trade-off between adversarial robustness and generalization by studying different models on ImageNet [78]. However, Su et al. compare the robustness and generalization characteristics of different models (i.e., different architectures, training strategies etc.), while we found that the generalization performance does not influence robustness for any *arbitrary, but fixed* model.

3.6. Discussion

Our results imply that robustness and generalization are not conflicting goals, as believed in related work [97, 90]:

Models can be both robust and accurate.

This means, in practice, for any arbitrary but fixed model, better generalization will not worsen off-manifold robustness. Different models (architectures, training strategies etc.) might, however, exhibit different robustness and generalization characteristics, as also shown in [90, 76]. For adversarial training, on regular adversarial examples, the commonly observed trade-off between robustness and generalization is explained by the tendency of adversarial examples to leave the manifold. As result, the network has to learn (seemingly) random, but adversarial, noise patterns *in addition* to the actual task at hand; rendering the learning problem harder. On simple datasets, such as EMNIST, these ad-

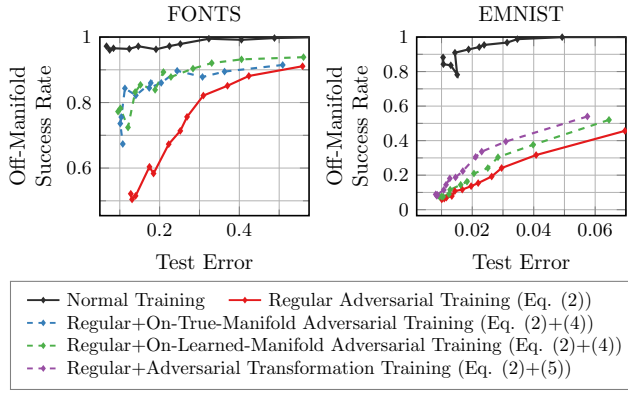


Figure 8: Adversarial training on regular adversarial examples, potentially leaving the manifold, renders the learning problem more difficult, as shown on FONTS and EMNIST, resulting in higher test error. This trade-off can be controlled by combining regular and on-manifold adversarial training. Test errors and success rates are averages over 3 models.

versarial directions might avoid overfitting; on harder tasks, e.g., FONTS or F-MNIST, the discrepancy in test error between normal and adversarial training increases. The trade-off is illustrated in Fig. 8 and can be controlled by combining regular and on-manifold adversarial training, i.e. boost generalization while reducing robustness.

The presented results can also be confirmed on more complex datasets, such as CelebA, and using different threat models, i.e., attacks. On CelebA, where VAE-GANs have difficulties approximating the manifold, Fig. 9 (top left) shows that on-manifold robustness still improves with generalization although most on-manifold adversarial examples are not very realistic, see Fig. 2. Similarly, regular robustness, see Fig. 9 (top right), is not influenced by generalization; here, we also show that the average distance of the perturbation, i.e., average $\|\delta\|_\infty$, when used to assess robustness leads to the same conclusions. Similarly, as shown in Fig. 9 (bottom), our findings are confirmed using Carlini and Wagner’s attack [14] with L_2 -norm – to show that the results generalize across norms. However, overall, we observed lower success rates using [14] and the L_2 norm. Finally, while white-box attacks are generally assumed to subsume black-box attacks (see, e.g., [6]), our results can also be reproduced using transfer attacks, as shown in the supplementary material.

4. Conclusion

In this paper, we intended to disentangle the relationship between adversarial robustness and generalization, by initially adopting the hypothesis that robustness and generalization are contradictory, i.e., both robust and accurate models are impossible [97, 90]. By considering adversarial examples in the context of the low-dimensional, underly-

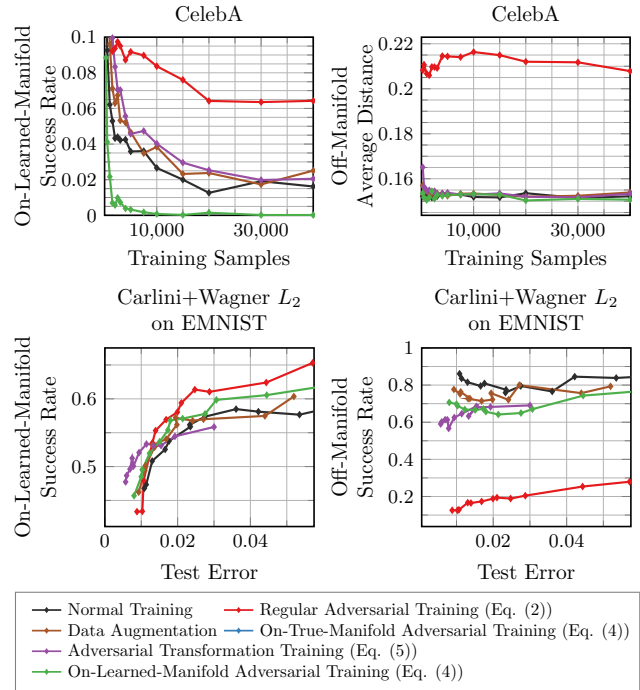


Figure 9: Our hypotheses can be confirmed on more complex datasets such as CelebA and different attacks such as Carlini and Wagner [14] using the L_2 norm. On CelebA, however, as the class manifolds are significantly harder to approximate, the benefit of on-manifold adversarial training diminishes. For [14], we increased the number of iterations to 120; our results are confirmed, although [14] does not use the training loss as attack objective and the L_2 norm changes the similarity-constraint for regular and on-manifold adversarial examples.

ing data manifold, we formulated and experimentally confirmed four assumptions. First, we showed that regular adversarial examples indeed leave the manifold, as widely assumed in related work [27, 94, 38, 72, 80]. Second, we demonstrated that adversarial examples can also be found on the manifold, so-called on-manifold adversarial examples; even if the manifold has to be approximated, e.g., using VAE-GANs [50, 74]. Third, we established that robustness against on-manifold adversarial examples is clearly related to generalization. Our proposed on-manifold adversarial training exploits this relationship to boost generalization using an approximate manifold, or known invariances. Fourth, we provided evidence that regular robustness, against regular, unconstrained adversarial examples, is independent of generalization; for any arbitrary but fixed model, better generalization, e.g., through more training data, does not reduce robustness. Altogether, these results imply that **adversarial robustness and generalization are not contradictory objectives**; at least our findings are in clear contradiction to the assumed hypothesis, meaning that both robust and accurate models are possible.

References

- [1] N. Akhtar and A. Mian. Threat of adversarial attacks on deep learning in computer vision: A survey. *arXiv.org*, abs/1801.00553, 2018. 2
- [2] R. Alaifari, G. S. Alberti, and T. Gauksson. Adef: an iterative algorithm to construct adversarial deformations. *arXiv.org*, abs/1804.07729, 2018. 6
- [3] M. Alzantot, Y. Sharma, A. Elgohary, B. Ho, M. B. Srivastava, and K. Chang. Generating natural language adversarial examples. In *EMNLP*, 2018. 2
- [4] L. Amsaleg, J. Bailey, D. Barbe, S. M. Erfani, M. E. Houle, V. Nguyen, and M. Radovanovic. The vulnerability of learning to adversarial perturbation increases with intrinsic dimensionality. In *WIFS*, 2017. 2
- [5] A. Athalye and N. Carlini. On the robustness of the CVPR 2018 white-box adversarial example defenses. *arXiv.org*, abs/1804.03286, 2018. 1, 2
- [6] A. Athalye, N. Carlini, and D. A. Wagner. Obfuscated gradients give a false sense of security: Circumventing defenses to adversarial examples. *arXiv.org*, abs/1802.00420, 2018. 1, 2, 5, 8
- [7] A. N. Bhagoji, D. Cullina, and P. Mittal. Dimensionality reduction as a defense against evasion attacks on machine learning classifiers. *arXiv.org*, abs/1704.02654, 2017. 2
- [8] A. N. Bhagoji, W. He, B. Li, and D. Song. Exploring the space of black-box attacks on deep neural networks. *arXiv.org*, abs/1712.09491, 2017. 1
- [9] B. Biggio and F. Roli. Wild patterns: Ten years after the rise of adversarial machine learning. *Pattern Recognition*, 84:317–331, 2018. 2
- [10] W. Brendel and M. Bethge. Comment on “biologically inspired protection of deep networks from adversarial attacks”. *arXiv.org*, abs/1704.01547, 2017. 2
- [11] T. B. Brown, N. Carlini, C. Zhang, C. Olsson, P. Christiano, and I. Goodfellow. Unrestricted adversarial examples. *arXiv.org*, abs/1809.08352, 2017. 1, 2
- [12] J. Buckman, A. Roy, C. Raffel, and I. Goodfellow. Thermometer encoding: One hot way to resist adversarial examples. In *ICLR*, 2018. 2
- [13] N. Carlini and D. Wagner. Adversarial examples are not easily detected: Bypassing ten detection methods. In *AISeC*, 2017. 2
- [14] N. Carlini and D. Wagner. Towards evaluating the robustness of neural networks. In *SP*, 2017. 2, 3, 4, 8, 12, 15, 16, 17
- [15] N. Carlini and D. A. Wagner. Defensive distillation is not robust to adversarial examples. *arXiv.org*, abs/1607.04311, 2016. 2
- [16] N. Carlini and D. A. Wagner. Audio adversarial examples: Targeted attacks on speech-to-text. In *SP*, 2018. 2
- [17] P.-Y. Chen, H. Zhang, Y. Sharma, J. Yi, and C.-J. Hsieh. ZOO: Zeroth order optimization based black-box attacks to deep neural networks without training substitute models. In *AISeC*, 2017. 2
- [18] M. M. Cisse, Y. Adi, N. Neverova, and J. Keshet. Houdini: Fooling deep structured visual and speech recognition models with adversarial examples. In *NIPS*, 2017. 2
- [19] G. Cohen, S. Afshar, J. Tapson, and A. van Schaik. EMNIST: an extension of MNIST to handwritten letters. *arXiv.org*, abs/1702.05373, 2017. 1, 2, 3, 12, 13
- [20] Y. Dong, F. Liao, T. Pang, H. Su, J. Zhu, X. Hu, and J. Li. Boosting adversarial attacks with momentum. In *CVPR*, 2018. 2, 15
- [21] L. Engstrom, D. Tsipras, L. Schmidt, and A. Madry. A rotation and a translation suffice: Fooling CNNs with simple transformations. *arXiv.org*, abs/1712.02779, 2017. 6
- [22] A. Fawzi, O. Fawzi, and P. Frossard. Fundamental limits on adversarial robustness. In *ICML Workshops*, 2015. 2
- [23] A. Fawzi, S.-M. Moosavi-Dezfooli, and P. Frossard. Robustness of classifiers: from adversarial to random noise. In *NIPS*, 2016. 18
- [24] A. Fawzi, H. Samulowitz, D. S. Turaga, and P. Frossard. Adaptive data augmentation for image classification. In *ICIP*, 2016. 3, 6
- [25] R. Feinman, R. R. Curtin, S. Shintre, and A. B. Gardner. Detecting adversarial samples from artifacts. *arXiv.org*, abs/1703.00410, 2017. 2
- [26] V. Fischer, M. C. Kumar, J. H. Metzen, and T. Brox. Adversarial examples for semantic image segmentation. *ICLR*, 2017. 2
- [27] J. Gilmer, L. Metz, F. Faghri, S. S. Schoenholz, M. Raghu, M. Wattenberg, and I. Goodfellow. Adversarial spheres. *ICLR Workshops*, 2018. 1, 2, 3, 5, 8
- [28] X. Glorot and Y. Bengio. Understanding the difficulty of training deep feedforward neural networks. In *AISTATS*, 2010. 3
- [29] I. J. Goodfellow, J. Pouget-Abadie, M. Mirza, B. Xu, D. Warde-Farley, S. Ozair, A. C. Courville, and Y. Bengio. Generative adversarial nets. In *NIPS*, 2014. 2
- [30] I. J. Goodfellow, J. Shlens, and C. Szegedy. Explaining and harnessing adversarial examples. *arXiv.org*, abs/1412.6572, 2014. 1, 2, 4, 18
- [31] K. Grosse, P. Manoharan, N. Papernot, M. Backes, and P. McDaniel. On the (statistical) detection of adversarial examples. *arXiv.org*, abs/1702.06280, 2017. 2
- [32] W. He, J. Wei, X. Chen, N. Carlini, and D. Song. Adversarial example defense: Ensembles of weak defenses are not strong. In *USENIX Workshops*, 2017. 2
- [33] M. Hein and M. Andriushchenko. Formal guarantees on the robustness of a classifier against adversarial manipulation. In *NIPS*, 2017. 2
- [34] R. Huang, B. Xu, D. Schuurmans, and C. Szepesvári. Learning with a strong adversary. *arXiv.org*, abs/1511.03034, 2015. 2, 4
- [35] S. H. Huang, N. Papernot, I. J. Goodfellow, Y. Duan, and P. Abbeel. Adversarial attacks on neural network policies. *ICLR*, 2017. 2
- [36] A. Ilyas, L. Engstrom, A. Athalye, and J. Lin. Black-box adversarial attacks with limited queries and information. In *ICML*, 2018. 1
- [37] A. Ilyas, L. Engstrom, and A. Madry. Prior convictions: Black-box adversarial attacks with bandits and priors. *arXiv.org*, abs/1807.07978, 2018. 2

- [38] A. Ilyas, A. Jalal, E. Asteri, C. Daskalakis, and A. G. Dimakis. The robust manifold defense: Adversarial training using generative models. *arXiv.org*, abs/1712.09196, 2017. 1, 2, 8
- [39] S. Ioffe and C. Szegedy. Batch normalization: Accelerating deep network training by reducing internal covariate shift. In *ICML*, 2015. 3, 13, 17
- [40] M. Jaderberg, K. Simonyan, A. Zisserman, and K. Kavukcuoglu. Spatial transformer networks. In *NIPS*, 2015. 3, 6, 13
- [41] D. Jakubovitz and R. Giryas. Improving DNN robustness to adversarial attacks using jacobian regularization. *arXiv.org*, abs/1803.08680, 2018. 2
- [42] M. Juuti, S. Szyller, A. Dmitrenko, S. Marchal, and N. Asokan. PRADA: Protecting against DNN model stealing attacks. *arXiv.org*, abs/1805.02628, 2018. 2
- [43] H. Kannan, A. Kurakin, and I. J. Goodfellow. Adversarial logit pairing. *arXiv.org*, abs/1803.06373, 2018. 2
- [44] D. P. Kingma and J. Ba. Adam: A method for stochastic optimization. *arXiv.org*, abs/1412.6980, 2014. 14
- [45] D. P. Kingma and J. Ba. Adam: A method for stochastic optimization. In *ICLR*, 2015. 3, 4, 13, 15, 16
- [46] D. P. Kingma and M. Welling. Auto-encoding variational bayes. In *ICLR*, 2014. 2, 13
- [47] J. Kos, I. Fischer, and D. Song. Adversarial examples for generative models. In *SP Workshops*, 2018. 2
- [48] A. Kurakin, I. Goodfellow, and S. Bengio. Adversarial examples in the physical world. *arXiv.org*, abs/1607.02533, 2016. 2
- [49] A. Lamb, J. Binas, A. Goyal, D. Serdyuk, S. Subramanian, I. Mitliagkas, and Y. Bengio. Fortified networks: Improving the robustness of deep networks by modeling the manifold of hidden representations. *arXiv.org*, abs/1804.02485, 2018. 2
- [50] A. B. L. Larsen, S. K. Sønderby, H. Larochelle, and O. Winther. Autoencoding beyond pixels using a learned similarity metric. In *ICML*, 2016. 3, 5, 8, 12, 13
- [51] Y. LeCun, L. Bottou, Y. Bengio, and P. Haffner. Gradient-based learning applied to document recognition. *Proceedings of the IEEE*, 86(11):2278–2324, 1998. 6
- [52] H. Lee, S. Han, and J. Lee. Generative adversarial trainer: Defense to adversarial perturbations with GAN. *arXiv.org*, abs/1705.03387, 2017. 2, 4
- [53] F. Liao, M. Liang, Y. Dong, T. Pang, X. Hu, and J. Zhu. Defense against adversarial attacks using high-level representation guided denoiser. In *CVPR*, 2018. 2
- [54] Y. Lin, Z. Hong, Y. Liao, M. Shih, M. Liu, and M. Sun. Tactics of adversarial attack on deep reinforcement learning agents. In *IJCAI*, 2017. 2
- [55] X. Liu, M. Cheng, H. Zhang, and C.-J. Hsieh. Towards robust neural networks via random self-ensemble. *arXiv.org*, abs/1712.00673, 2017. 2
- [56] Y. Liu, X. Chen, C. Liu, and D. Song. Delving into transferable adversarial examples and black-box attacks. *arXiv.org*, abs/1611.02770, 2016. 1
- [57] Y. Liu, X. Chen, C. Liu, and D. Song. Delving into transferable adversarial examples and black-box attacks. *ICLR*, 2017. 2, 16
- [58] Z. Liu, P. Luo, X. Wang, and X. Tang. Deep learning face attributes in the wild. In *ICCV*, 2015. 1, 2, 3, 13
- [59] B. Luo, Y. Liu, L. Wei, and Q. Xu. Towards imperceptible and robust adversarial example attacks against neural networks. In *AAAI*, 2018. 2
- [60] X. Ma, B. Li, Y. W. adn Sarah M. Erfani, S. Wijewickrema, M. E. Houle, G. Schoenebeck, D. Song, and J. Bailey. Characterizing adversarial subspaces using local intrinsic dimensionality. *arXiv.org*, abs/1801.02613, 2018. 2
- [61] A. Madry, A. Makelov, L. Schmidt, D. Tsipras, and A. Vladu. Towards deep learning models resistant to adversarial attacks. *arXiv.org*, abs/1706.06083, 2017. 2
- [62] A. Madry, A. Makelov, L. Schmidt, D. Tsipras, and A. Vladu. Towards deep learning models resistant to adversarial attacks. *ICLR*, 2018. 1, 4, 12, 14, 15, 16, 17, 18
- [63] J. H. Metzen, T. Genewein, V. Fischer, and B. Bischoff. On detecting adversarial perturbations. *arXiv.org*, abs/1702.04267, 2017. 2
- [64] T. Miyato, S.-i. Maeda, S. Ishii, and M. Koyama. Virtual adversarial training: a regularization method for supervised and semi-supervised learning. *PAMI*, 2018. 3
- [65] T. Miyato, S.-i. Maeda, M. Koyama, K. Nakae, and S. Ishii. Distributional smoothing with virtual adversarial training. *ICLR*, 2016. 2, 3, 4
- [66] S. Moosavi-Dezfooli, A. Fawzi, and P. Frossard. Deepfool: A simple and accurate method to fool deep neural networks. In *CVPR*, 2016. 2
- [67] N. Narodytska and S. P. Kasiviswanathan. Simple black-box adversarial attacks on deep neural networks. In *CVPR Workshops*, 2017. 2
- [68] A. Nayebi and S. Ganguli. Biologically inspired protection of deep networks from adversarial attacks. *arXiv.org*, abs/1703.09202, 2017. 2
- [69] S. J. Oh, M. Augustin, M. Fritz, and B. Schiele. Towards reverse-engineering black-box neural networks. *ICLR*, 2018. 2
- [70] N. Papernot, P. McDaniel, I. Goodfellow, S. Jha, Z. B. Celik, and A. Swami. Practical black-box attacks against machine learning. In *AsiaCCS*. ACM, 2017. 2, 16
- [71] N. Papernot, P. D. McDaniel, S. Jha, M. Fredrikson, Z. B. Celik, and A. Swami. The limitations of deep learning in adversarial settings. In *SP*, 2016. 2
- [72] R. C. Pouya Samangouei, Maya Kabkab. Defense-GAN: Protecting classifiers against adversarial attacks using generative models. *ICLR*, 2018. 1, 2, 8
- [73] A. Prakash, N. Moran, S. Garber, A. DiLillo, and J. A. Storer. Protecting JPEG images against adversarial attacks. In *DCC*, 2018. 2
- [74] M. Rosca, B. Lakshminarayanan, D. Warde-Farley, and S. Mohamed. Variational approaches for auto-encoding generative adversarial networks. *arXiv.org*, abs/1706.04987, 2017. 3, 5, 8, 12, 13
- [75] A. S. Ross and F. Doshi-Velez. Improving the adversarial robustness and interpretability of deep neural networks by regularizing their input gradients. In *AAAI*, 2018. 2
- [76] A. Rozsa, M. Günther, and T. E. Boulton. Are accuracy and robustness correlated. In *ICMLA*, 2016. 2, 7

- [77] A. Rozsa, M. Günther, and T. E. Boult. Adversarial robustness: Softmax versus openmax. In *BMVC*, 2017. 2
- [78] O. Russakovsky, J. Deng, H. Su, J. Krause, S. Satheesh, S. Ma, Z. Huang, A. Karpathy, A. Khosla, M. S. Bernstein, A. C. Berg, and F. Li. Imagenet large scale visual recognition challenge. *IJCV*, 115(3):211–252, 2015. 2, 7
- [79] S. Sarkar, A. Bansal, U. Mahbub, and R. Chellappa. UPSET and ANGRI : Breaking high performance image classifiers. *arXiv.org*, abs/1707.01159, 2017. 2
- [80] L. Schott, J. Rauber, W. Brendel, and M. Bethge. Robust perception through analysis by synthesis. *arXiv.org*, abs/1805.09190, 2018. 1, 2, 5, 8
- [81] U. Shaham, Y. Yamada, and S. Negahban. Understanding adversarial training: Increasing local stability of supervised models through robust optimization. *Neurocomputing*, 307:195–204, 2018. 2, 4
- [82] M. Sharif, L. Bauer, and M. K. Reiter. On the suitability of l_p -norms for creating and preventing adversarial examples. *arXiv.org*, abs/1802.09653, 2018. 2
- [83] Y. Sharma and P.-Y. Chen. Attacking the madry defense model with l_1 -based adversarial examples. *arXiv.org*, abs/1710.10733, 2017. 2
- [84] S. Shen, G. Jin, K. Gao, and Y. Zhang. Ape-gan: Adversarial perturbation elimination with gan. *arXiv.org*, abs/1707.05474, 2017. 2
- [85] R. Shokri, M. Stronati, C. Song, and V. Shmatikov. Membership inference attacks against machine learning models. In *SP*, 2017. 2
- [86] C.-J. Simon-Gabriel, Y. Ollivier, B. Schölkopf, L. Bottou, and D. Lopez-Paz. Adversarial vulnerability of neural networks increases with input dimension. *arXiv.org*, abs/1802.01421, 2018. 2
- [87] A. Sinha, H. Namkoong, and J. C. Duchi. Certifiable distributional robustness with principled adversarial training. *ICLR*, 2018. 2, 4
- [88] Y. Song, R. Shu, N. Kushman, and S. Ermon. Generative adversarial examples. *arXiv.org*, abs/1805.07894, 2018. 1, 2
- [89] T. Strauss, M. Hanselmann, A. Junginger, and H. Ulmer. Ensemble methods as a defense to adversarial perturbations against deep neural networks. *arXiv.org*, abs/1709.03423, 2017. 2
- [90] D. Su, H. Zhang, H. Chen, J. Yi, P.-Y. Chen, and Y. Gao. Is robustness the cost of accuracy? – a comprehensive study on the robustness of 18 deep image classification models. *arXiv.org*, abs/1808.01688, 2018. 1, 2, 3, 7, 8
- [91] J. Su, D. V. Vargas, and K. Sakurai. One pixel attack for fooling deep neural networks. *arXiv.org*, abs/1710.08864, 2017. 2
- [92] C. Szegedy, W. Zaremba, I. Sutskever, J. Bruna, D. Erhan, I. Goodfellow, and R. Fergus. Intriguing properties of neural networks. *arXiv.org*, abs/1312.6199, 2013. 1, 2, 4, 18
- [93] P. Tabacof, J. Tavares, and E. Valle. Adversarial images for variational autoencoders. *arXiv.org*, abs/1612.00155, 2016. 2
- [94] T. Tanay and L. Griffin. A boundary tilting perspective on the phenomenon of adversarial examples. *arXiv.org*, abs/1608.07690, 2016. 1, 2, 8
- [95] F. Tramèr, A. Kurakin, N. Papernot, D. Boneh, and P. D. McDaniel. Ensemble adversarial training: Attacks and defenses. *ICLR*, 2018. 2
- [96] F. Tramèr, F. Zhang, A. Juels, M. K. Reiter, and T. Ristenpart. Stealing machine learning models via prediction apis. In *USENIX*, 2016. 2
- [97] D. Tsipras, S. Santurkar, L. Engstrom, A. Turner, and A. Madry. Robustness may be at odds with accuracy. *arXiv.org*, abs/1805.12152, 2018. 1, 2, 3, 7, 8, 12, 18, 19
- [98] B. Wang and N. Z. Gong. Stealing hyperparameters in machine learning. In *SP*, 2018. 2
- [99] Y. Wang, S. Jha, and K. Chaudhuri. Analyzing the robustness of nearest neighbors to adversarial examples. In *ICML*, 2018. 2
- [100] C. Xiao, J. Zhu, B. Li, W. He, M. Liu, and D. Song. Spatially transformed adversarial examples. *ICLR*, 2018. 6
- [101] H. Xiao, K. Rasul, and R. Vollgraf. Fashion-MNIST: a novel image dataset for benchmarking machine learning algorithms. *arXiv.org*, abs/1708.07747, 2017. 1, 2, 3, 13
- [102] C. Xie, J. Wang, Z. Zhang, Z. Ren, and A. L. Yuille. Mitigating adversarial effects through randomization. *ICLR*, 2018. 2
- [103] C. Xie, Z. Zhang, J. Wang, Y. Zhou, Z. Ren, and A. L. Yuille. Improving transferability of adversarial examples with input diversity. *arXiv.org*, abs/1803.06978, 2018. 2, 16
- [104] X. Yuan, P. He, Q. Zhu, R. R. Bhat, and X. Li. Adversarial examples: Attacks and defenses for deep learning. *arXiv.org*, abs/1712.07107, 2017. 2
- [105] V. Zantedeschi, M.-I. Nicolae, and A. Rawat. Efficient defenses against adversarial attacks. In *AISeC*, 2017. 2, 4
- [106] Z. Zhao, D. Dua, and S. Singh. Generating natural adversarial examples. *arXiv.org*, abs/1710.11342, 2017. 1
- [107] Z. Zhao, D. Dua, and S. Singh. Generating natural adversarial examples. *ICLR*, 2018. 2, 3, 5

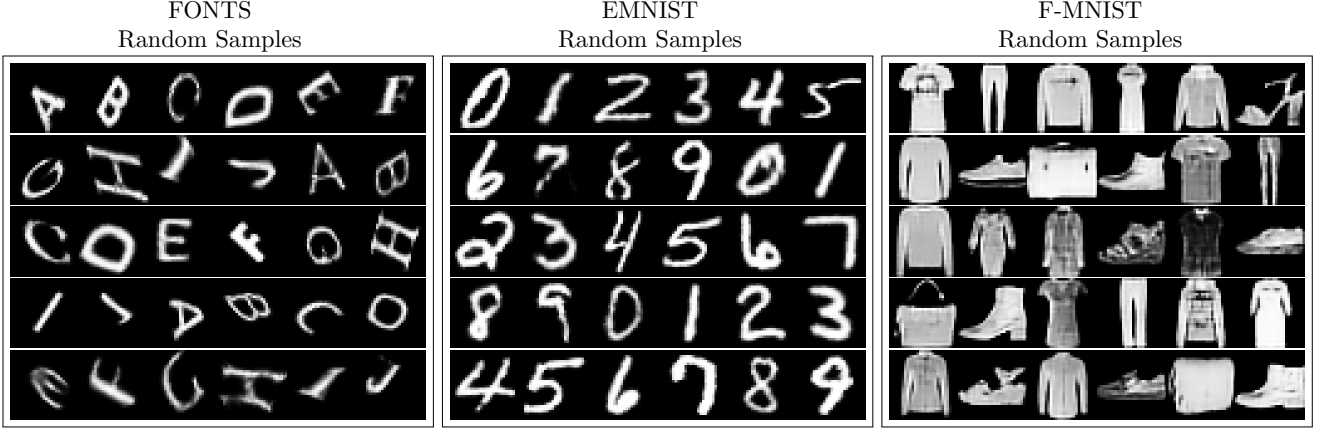


Figure 10: For FONTS (left), EMNIST (middle) and F-MNIST (right), we show random samples from the learned, class-specific VAE-GANs used to craft on-manifold adversarial examples. Our VAE-GANs generate realistic looking samples; although we also include problematic samples illustrating the discrepancy between true and approximated data distribution.

A. Overview

In the main paper, we study the relationship between adversarial robustness and generalization. Based on the distinction between regular and on-manifold adversarial examples, we show that 1. regular adversarial examples leave the underlying manifold of the data; 2. on-manifold adversarial examples exist; 3. on-manifold robustness is essentially generalization; 4. and regular robustness is independent of generalization. For clarity and brevity, the main paper focuses on the L_∞ attack by Madry et al. [62] and the corresponding adversarial training variant applied to simple convolutional neural networks. For on-manifold adversarial examples, we approximate the manifold using class-specific VAE-GANs [50, 74]. In this document, we present comprehensive experiments demonstrating that our findings generalize across attacks, adversarial training variants, network architectures and to class-agnostic VAE-GANs.

A.1. Contents

In Section B, we present additional details regarding our experimental setup, corresponding to Section 3.1 of the main paper: in Section B.1, we discuss details of our synthetic FONTS datasets and, in Section B.2, we discuss our VAE-GAN implementation. Then, in Section C we extend the discussion of Section 3.2 with further results demonstrating that adversarial examples leave the manifold. Subsequently, in Section D, we show and discuss additional on-manifold adversarial examples to supplement the examples shown in Fig. 2 of the main paper. Then, complementing the discussion in Section 3.4 and 3.5, we consider additional attacks, network architectures and class-agnostic VAE-GANs. Specifically, in Section E, we consider the L_2 variant of the white-box attack by Madry et al. [62], the L_2 white-box attack by Carlini and Wagner [14], and black-box

transfer attacks. In Section F, we present experiments on multi-layer perceptrons and, in Section G, we consider approximating the manifold using class-agnostic VAE-GANs. In Section H, corresponding to Section 3.6, we consider different variants of regular and on-manifold adversarial training. Finally, in Section I, we discuss our definition of adversarial examples in the context of related work by Tsipras et al. [97], as outlined in Section 3.5.

B. Experimental Setup

We provide technical details on the introduced synthetic FONTS dataset, Section B.1, and our VAE-GAN implementation, Section B.2.

B.1. FONTS Dataset

Our FONTS dataset consists of randomly rotated characters “A” to “J” from different fonts, as outlined in Section 3.1 of the main paper. Specifically, we consider 1000 Google Fonts as downloaded from the corresponding GitHub repository². We manually exclude fonts based on symbols, or fonts that could not be rendered correctly in order to obtain a cleaned dataset consisting of clearly readable letters “A” to “J”; still, the 1000 fonts exhibit significant variance. The obtained, rendered letters are transformed using translation, shear, scaling and rotation: for each letter and font, we create 112 transformations, uniformly sampled in $[-0.2, 0.2]$, $[-0.5, 0.5]$, $[0.75, 1.15]$, and $[-\pi/2, \pi/2]$, respectively. As a result, with 1000 fonts and 10 classes, we obtain 1.12Mio images of size 28×28 , splitted into 960k training images and 160k test images (of which we use 40k in the main paper); thus, the dataset has four times the size of EMNIST [19]. For simplicity, the transformations are

²<https://github.com/google/fonts>

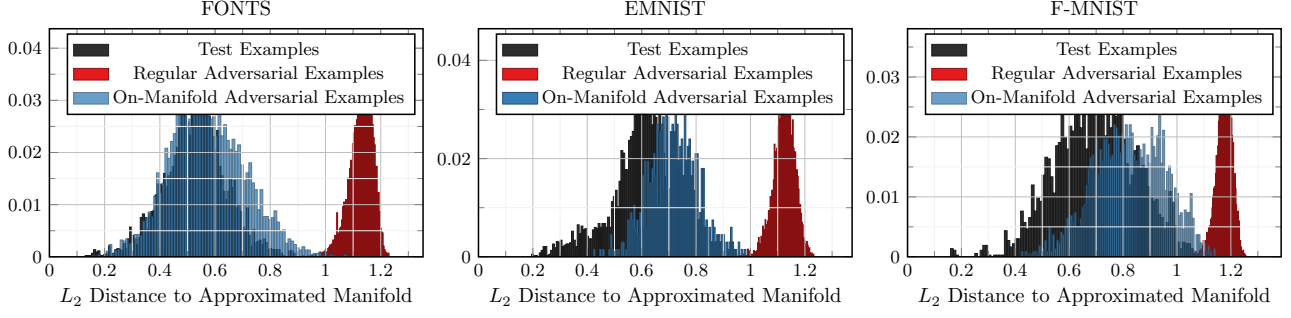


Figure 11: On FONTs (left), EMNIST (middle) and F-MNIST (right) we plot the distance of adversarial examples to the approximated manifold. We show normalized histograms of the L_2 distance of adversarial examples to their projection, as described in the text. Regular adversarial examples exhibit a significant distance to the manifold; clearly distinguishable from on-manifold adversarial examples and test images. We also note that, depending on the VAE-GAN approximation, on-manifold adversarial examples are hardly distinguishable from test images.

applied using a spatial transformer network [40] by assembling translation $[t_1, t_2]$, shear $[\lambda_1, \lambda_2]$, scale s and rotation r into an affine transformation matrix,

$$\begin{bmatrix} \cos(r)s - \sin(r)s\lambda_1 & -\sin(r)s + \cos(r)s\lambda_1 & t_1 \\ \cos(r)s\lambda_2 + \sin(r)s & -\sin(r)s\lambda_2 + \cos(r)s & t_2 \end{bmatrix}, \quad (6)$$

making the generation process fully differentiable. Overall, FONTs offers full control over the manifold, i.e., the transformation parameters, font and class, with differentiable generative model, i.e., decoder.

B.2. VAE-GAN Variant

As briefly outlined in Section 3.1 of the main paper, we use class-specific VAE-GANs [50, 74] to approximate the class-manifolds on all datasets, i.e., FONTs, EMNIST [19], F-MNIST [101] and CelebA [58]. In contrast to [50], however, we use a reconstruction loss on the image, not on the discriminator’s features; in contrast to [74], we use the standard Kullback-Leibler divergence to regularize the latent space. The model consists of an encoder enc , approximating the posterior $q(z|x) \approx p(z|x)$ of latent code z given image x , a (deterministic) decoder dec , and a discriminator dis . During training, the sum of the following losses is minimized:

$$\mathcal{L}_{\text{enc}} = \mathbb{E}_{q(z|x)} [\lambda \|x - \text{dec}(z)\|_1] + \text{KL}(q(z|x)|p(z)) \quad (7)$$

$$\mathcal{L}_{\text{dec}} = \mathbb{E}_{q(z|x)} [\lambda \|x - \text{dec}(z)\|_1 - \log(\text{dis}(\text{dec}(z)))] \quad (8)$$

$$\begin{aligned} \mathcal{L}_{\text{dis}} = & -\mathbb{E}_{p(x)} [\log(\text{dis}(x))] \\ & -\mathbb{E}_{q(z|x)} [\log(1 - \text{dis}(\text{dec}(z)))] \end{aligned} \quad (9)$$

using a standard Gaussian prior $p(z)$. Here, $q(z|x)$ is modeled by predicting the mean $\mu(x)$ and variance $\sigma^2(x)$ such that $q(z|x) = \mathcal{N}(z; \mu(x), \text{diag}(\sigma^2(x)))$ and the weighting parameter λ controls the importance of the L_1 reconstruction loss relative to the Kullback-Leibler divergence KL and the adversarial loss for decoder and discriminator. As in [46], we use the reparameterization trick with one sample to approximate the expectations in Eq. (7), (8) and (9), and

the Kullback-Leibler divergence $\text{KL}(q(z|x)|p(z))$ is computed analytically.

The encoder, decoder and discriminator consist of three (four for CelebA) (de-) convolutional layers (4×4 kernels; stride 2; 64, 128, 256 channels), followed by ReLU activations and batch normalization [39]; the encoder uses two fully connected layers to predict mean and variance; the discriminator uses two fully connected layers to predict logits. We tuned λ to dataset- and class-specific values: on FONTs, $\lambda = 3$ worked well for all classes, on EMNIST, $\lambda = 2.5$ except for classes “0” ($\lambda = 2.75$), “1” ($\lambda = 5.6$) and “8” ($\lambda = 2.25$), on F-MNIST, $\lambda = 2.75$ worked well for all classes, on CelebA $\lambda = 3$ worked well for both classes. Finally, we trained our VAE-GANs using ADAM [45] with learning rate 0.005 (decayed by 0.9 every epoch), weight decay 0.0001 and batch size 100 for 10, 30, 60 and 30 epochs on FONTs, EMNIST, F-MNIST and CelebA, respectively. We also consider class-agnostic VAE-GANs trained using the same strategy with $\lambda = 3$ for FONTs, $\lambda = 3$ on EMNIST, $\lambda = 2.75$ on F-MNIST and $\lambda = 3$ on CelebA, see Section G for results.

In Fig. 10, we include random samples of the class-specific VAE-GANs. Especially on EMNIST and FONTs, our VAE-GANs generate realistic looking samples with sharp edges. However, we also show several problematic random samples, illustrating the discrepancy between the true data distribution and the approximation – as particularly highlighted on FONTs.

C. Adversarial Example Distance to Manifold

Complementing Section 3.2 of the main paper, we provide additional details and results regarding the distance of regular adversarial examples to the true or approximated manifold.

On FONTs, with access to the true manifold in form of a perfect decoder dec , we iteratively obtain the latent code \tilde{z} yielding the manifold’s closest image to the given adver-

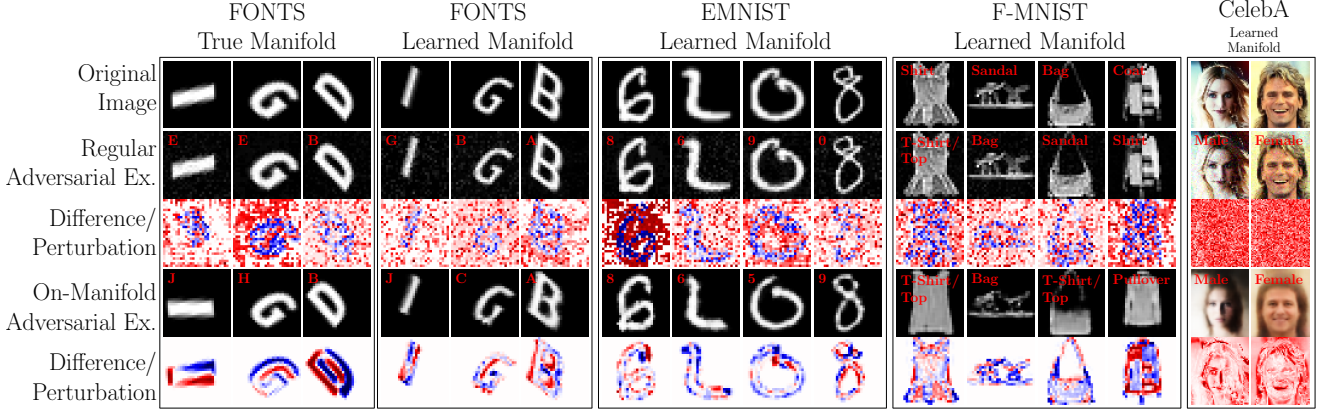


Figure 12: Regular and on-manifold adversarial examples on FONTS, EMNIST, F-MNIST and CelebA. On FONTS, the manifold is known; on the other datasets, class manifolds have been approximated using VAE-GANs. Notice that the crafted on-manifold adversarial examples correspond to meaningful manipulations of the image – as long as the learned class-manifolds are good approximations. This can best be seen considering the (normalized) difference images (or the magnitude thereof for CelebA).

sarial example \tilde{x} as

$$\tilde{z} = \underset{z}{\operatorname{argmin}} \|\tilde{x} - \operatorname{dec}(z)\|_2^2. \quad (10)$$

We use 100 iterations of ADAM [44], with a learning rate of 0.09, decayed every 10 iterations by a factor 0.95. We found that additional iterations did not improve the results. The obtained projection $\pi(\tilde{x}) = \operatorname{dec}(\tilde{z})$ is usually very close to the original test image x for which the adversarial example was crafted. The distance is then computed as $\|\tilde{x} - \pi(\tilde{x})\|_2$; we refer to the main paper for results and discussion.

If the true manifold is not available, we locally approximate the manifold using 50 nearest neighbors x_1, \dots, x_{50} of the adversarial example \tilde{x} . In the main paper, we center these nearest neighbors at the test image x , i.e., consider the sub-space spanned by $x_i - x$. Here, we show that the results can be confirmed when centering the nearest neighbors at their mean $\bar{x} = 1/50 \sum_{i=1}^{50} x_i$ and considering the subspace spanned by $x_i - \bar{x}$ instead. In this scenario, the test image x is not necessarily part of the approximated manifold anymore. The projection onto this sub-space can be obtained by solving the least squares problem; specifically, we consider the vector $\delta = \tilde{x} - x$, i.e., we assume that the “adversarial direction” originates at the mean \bar{x} . Then, we solve

$$\beta^* = \underset{\beta}{\operatorname{argmin}} \|X\beta - \delta\|_2^2 \quad (11)$$

where the columns X_i are the vectors $x_i - \bar{x}$. The projection $\pi(\tilde{x})$ is obtained as $\pi(\tilde{x}) = X\beta^*$; the same approach can be applied to projecting the test image x . Note that it is crucial to consider the adversarial direction δ itself, instead of the adversarial example \tilde{x} because $\|\delta\|_2$ is small by construction, i.e., the projections of \tilde{x} and x are very close. In Fig. 11, we show results using this approximation on FONTS, EMNIST and F-MNIST. Regular adversarial examples can clearly be distinguished from test images and

on-manifold adversarial examples. Note, however, that we assume access to both the test image x and the corresponding adversarial example \tilde{x} such that this finding cannot be exploited for detection. We also notice that the discrepancy between the distance distributions of test images and on-manifold adversarial examples reflects the approximation quality of the used VAE-GANs.

D. On-Manifold Adversarial Examples

In Fig. 12, we show additional examples of regular and on-manifold adversarial examples, complementing the examples in Fig. 2 of the main paper. On FONTS, both using the true and the approximated manifold, on-manifold adversarial examples reflect the underlying invariances of the data, i.e., the transformations employed in the generation process. This is in contrast to the corresponding regular adversarial examples and their (seemingly) random noise patterns. We note that regular and on-manifold adversarial examples can best be distinguished based on their difference to the original test image – although both are perceptually close to the original image. Similar observations hold on EMNIST and F-MNIST. However, especially on F-MNIST and CelebA, the discrepancy between true images and on-manifold adversarial examples becomes visible. This is the “cost” of approximating the underlying manifold using VAE-GANs. More examples can be found in Fig. 20 at the end of this document.

E. L_2 and Transfer Attacks

In the main paper, see Section 3.1, we primarily focus on the L_∞ white-box attack by Madry et al. [62]. Here, we further consider the L_2 variant, which, given image x with label y and classifier f , maximizes the training loss, i.e.,

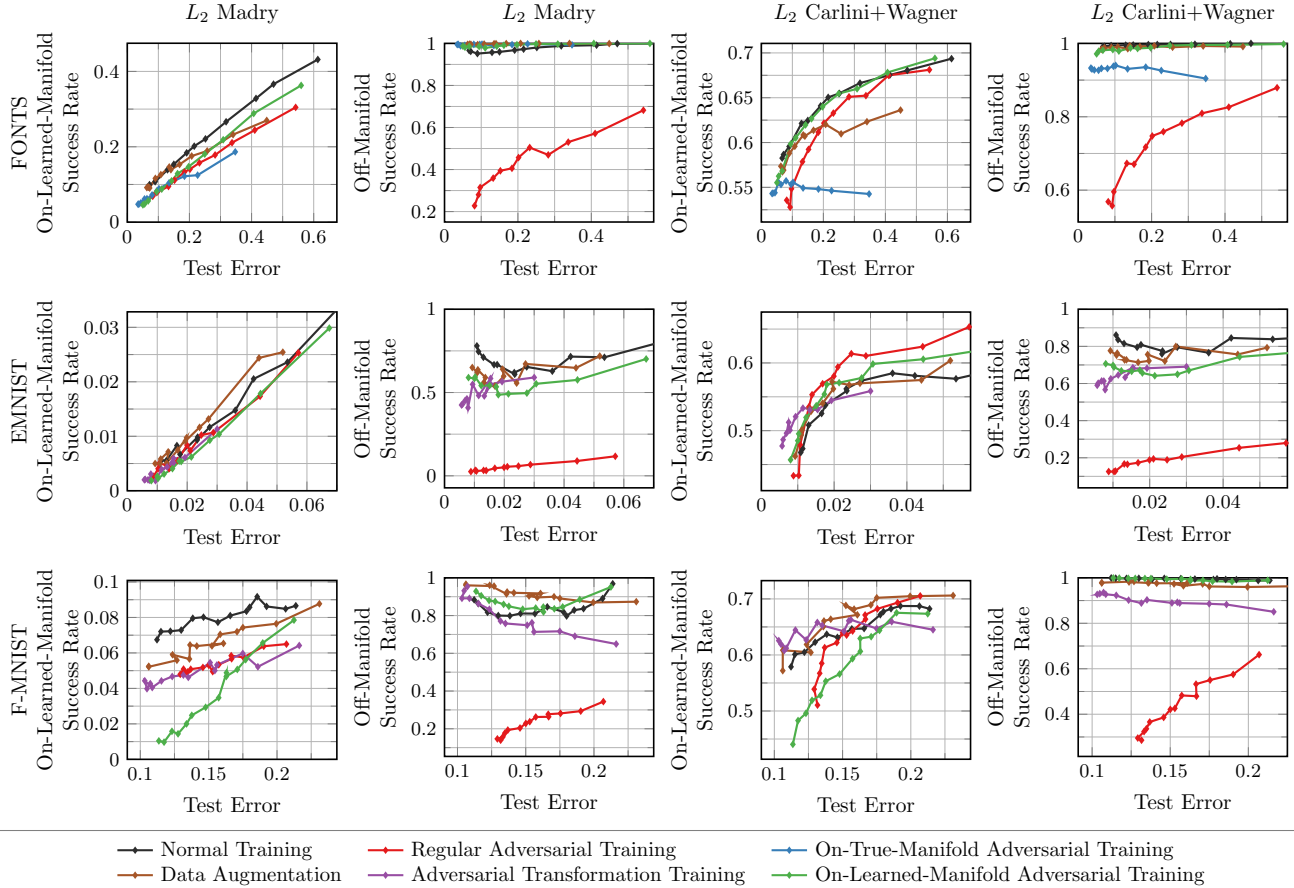


Figure 13: L_2 attacks of Madry et al. [62] and Carlini and Wagner [14] on FONTS, EMNIST and F-MNIST. In all cases, we plot regular or on-manifold success rate against test error. Independent of the attack, we can confirm that on-manifold robustness is strongly related to generalization, while regular robustness is independent of generalization.

$$\max_{\delta} \mathcal{L}(f(x + \delta), y) \text{ s.t. } \|\delta\|_2 \leq \epsilon, \tilde{x}_i \in [0, 1], \quad (12)$$

to obtain an adversarial example $\tilde{x} = x + \delta$. We use projected ADAM [45]: after each iteration, \tilde{x} is projected onto the L_2 -ball of radius ϵ using

$$\tilde{x}' = \tilde{x} \cdot \max\left(1, \frac{\epsilon}{\|\tilde{x}\|_2}\right) \quad (13)$$

and clipped to $[0, 1]$. We use a learning rate of 0.005 and we note that ADAM includes momentum, as suggested in [20]. Optimization stops as soon as the label changes, or runs for a maximum of 40 iterations. The perturbation δ is initialized randomly as follows:

$$\delta = u\epsilon \frac{\delta'}{\|\delta'\|_2}, \quad \delta' \sim \mathcal{N}(0, I), u \sim U(0, 1). \quad (14)$$

Here, $U(0, 1)$ refers to the uniform distribution over $[0, 1]$. This results in δ being in the ϵ -ball and uniformly distributed over distance and direction. Note that this is in contrast to sampling uniformly wrt. the volume of the ϵ -ball. The

same procedure applies to the L_∞ attack where the projection onto the ϵ -ball is achieved by clipping. The attack can also be used to obtain on-manifold adversarial examples, as described in Section 3.3 of the main paper. Then, optimization in Eq. (12) is done over the perturbation ζ in latent space, with constraint $\|\zeta\|_2 \leq \eta$. The adversarial example is obtained as $\tilde{x} = \text{dec}(z + \zeta)$ with z being the latent code of image x and dec being the true or approximated generative model, i.e., decoder.

We also consider the L_2 white box attack by Carlini and Wagner [14]. Instead of directly maximizing the training loss, Carlini and Wagner propose to use a surrogate objective on the classifier's logits l_y :

$$F(\tilde{x}, y) = \max(-\kappa, l_y(\tilde{x}) - \max_{y' \neq y} l_{y'}(\tilde{x})). \quad (15)$$

Compared to the training loss, which might be close to zero for a well-trained network, F is argued to provide more useful gradients [14]. Then,

$$\min_{\delta} F(x + \delta, y) + \lambda \|\delta\|_2 \text{ s.t. } \tilde{x}_i \in [0, 1] \quad (16)$$

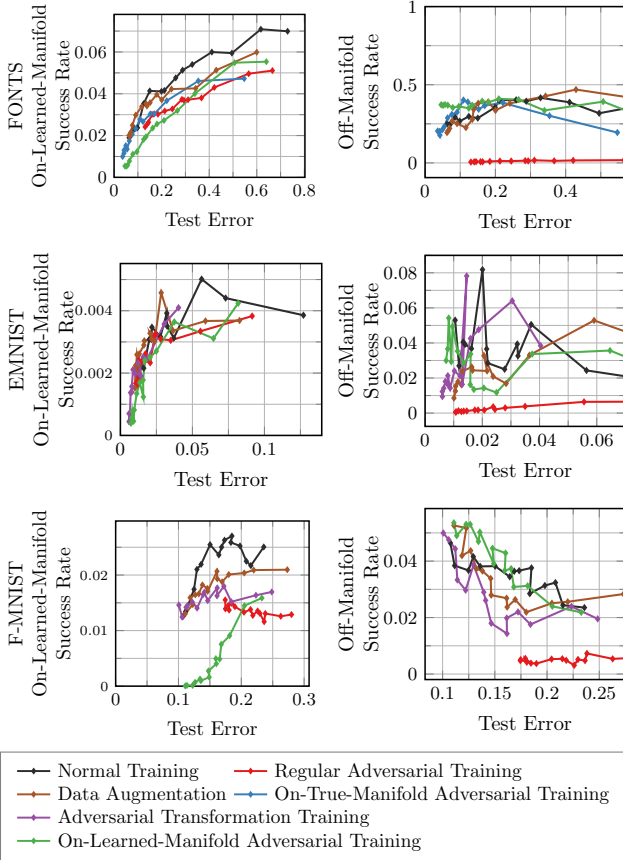


Figure 14: Transfer attacks on FONTS, EMNIST and F-MNIST. We show on-manifold (left) and regular success rate (right) plotted against test error. In spite of significantly lower success rates, transfer attacks also allow to confirm the strong relationship between on-manifold success rate and test error, while – at least on FONTS and EMNIST – regular success rate is independent of test error.

is minimized by reparameterizing δ in terms of $\delta = 1/2(\tanh(\omega)+1)-x$ in order to ensure the image-constraint, i.e., $\tilde{x}_i \in [0, 1]$. In practice, we empirically chose $\kappa = 1.5$, use 120 iterations of ADAM [45] with learning rate 0.005 and $\lambda = 1$. Again, this attack can be used to obtain on-manifold adversarial examples, as well.

As black-box attack we transfer L_∞ Madry adversarial examples from a held out model, as previously done in [57, 103, 70]. The held out transfer model is trained normally, i.e., without any data augmentation or adversarial training, on 10k training images for 20 epochs (as outlined in Section 3.1 of the main paper). The success rate of these transfer attacks is computed with respect to images that are correctly classified by both the transfer model and the target model.

Extending the discussion of Section 3.4 and 3.5 of the main paper, Fig. 13 shows results on FONTS, EMNIST and F-MNIST considering both L_2 attacks, i.e., Madry et al.

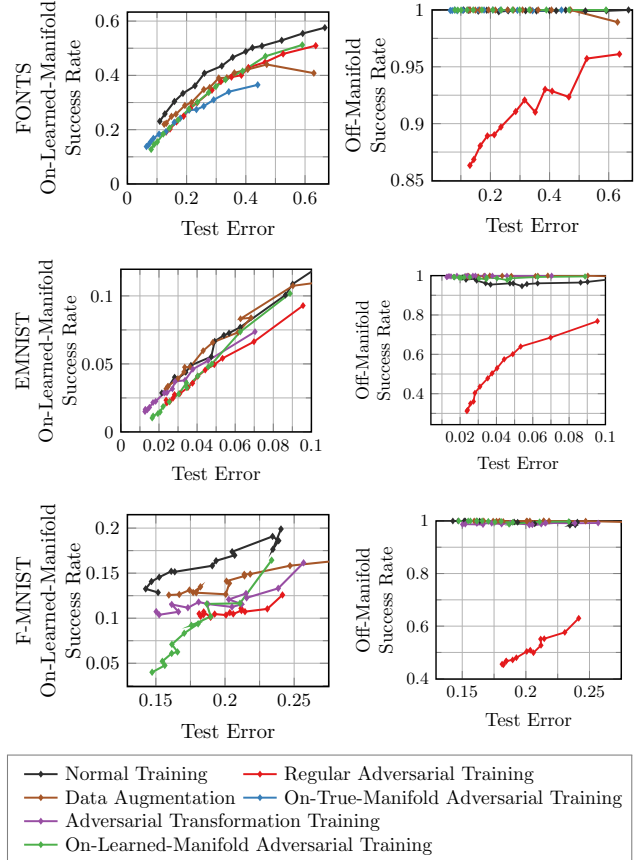


Figure 15: Experiments with multilayer-perceptrons on FONTS, EMNIST and F-MNIST. We plot on-manifold (left) or regular success rate (right) against test error. On-manifold robustness is strongly related to generalization, while regular robustness seems mostly independent of generalization.

[62] and Carlini and Wagner [14]. In contrast to the L_∞ Madry attack, we observe generally lower success rates. Nevertheless, we can observe a clear relationship between on-manifold success rate and test error. The exact form of this relationship, however, depends on the attack; for the L_2 Madry attack, the relationships seems to be mostly linear (especially on FONTS and EMNIST), while it seems non-linear for the L_2 Carlini and Wagner attack. Furthermore, the independence of regular robustness and generalization can be confirmed, i.e., regular success rate is roughly constant when test error varies – again, with the exception of regular adversarial training.

In Fig. 14, we also consider the black-box case, i.e., without access to the target model. While both observations from above can be confirmed, especially on FONTS and EMNIST, the results are significantly less pronounced. This is mainly due to the significantly lower success rate of transfer attacks – both regarding regular and on-manifold adversarial examples. Especially on EMNIST and F-MNIST,

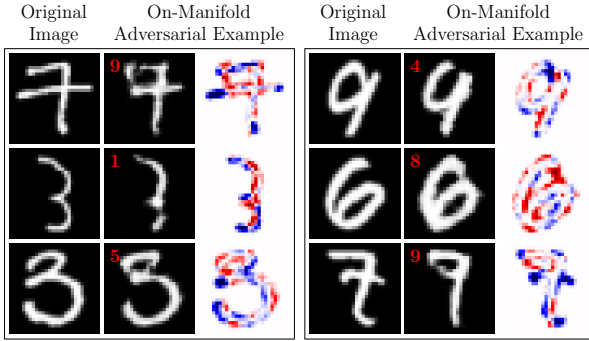


Figure 16: On-manifold adversarial examples crafted using class-agnostic VAE-GANs on EMNIST. We show examples illustrating the problematic of unclear class boundaries within the learned manifold. On-manifold adversarial examples are not guaranteed to be label invariant, i.e., they may change the actual, true label according to the approximate data distribution.

success rate may reduce from previously 80% or higher to 10% or lower. This might also explain the high variance on EMNIST and F-MNIST regarding regular robustness. Overall, we demonstrate that our claims can be confirmed in both white- and black-box settings as well as using different attacks [62, 14] and norms.

F. Influence of Network Architecture

Also in relation to the discussion in Section 3.4 and 3.5 of the main paper, Fig. 15 shows results on FONTS, EMNIST and F-MNIST using multi-layer perceptrons instead of convolutional neural networks. Specifically, we consider a network with 4 hidden layers, using 128 hidden units each; each layer is followed by ReLU activations and batch normalization [39]; training strategy, however, remains unchanged. Both of our claims, i.e., that on-manifold robustness is essentially generalization but regular robustness is independent of generalization, can be confirmed. Especially regarding the latter, results are more pronounced using multi-layer perceptrons: except for regular adversarial training, success rate stays nearly constant at 100% irrespective of test error. Overall, these results suggest that our claims generally hold for the class of (deep) neural networks, irrespective of architectural details.

G. From Class Manifolds to Data Manifold

In the context of Section 3.3 and 3.4 of the main paper, we consider approximating the manifold using class-agnostic VAE-GANs. Instead of the class-conditionals $p(x|y)$ of the data distribution, the marginals $p(x)$ are approximated, i.e., images of different classes are embedded in the same latent space. Then, however, ensuring label invariance, as required by our definition of on-manifold adversarial examples, becomes difficult:

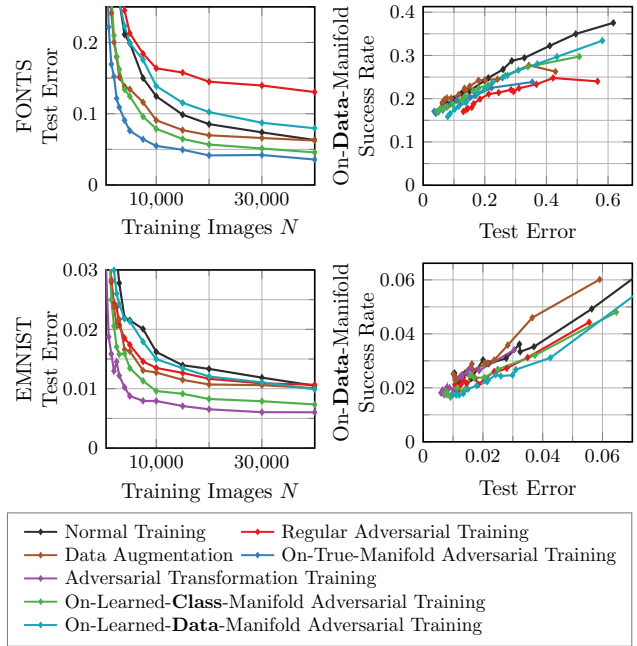


Figure 17: Test error and on-data-manifold success rate on FONTS and EMNIST. Using class-agnostic VAE-GANs, without clear class boundaries, on-manifold adversarial training loses its effectiveness – the on-manifold adversarial examples cross the true class boundaries too often. The strong relationship between on-manifold robustness and generalization can still be confirmed.

Definition 2 (On-Manifold Adversarial Example). Given the data distribution p , an on-manifold adversarial example for x with label y is a perturbed version \tilde{x} such that $f(\tilde{x}) \neq y$ but $p(y|\tilde{x}) > p(y'|\tilde{x}) \forall y' \neq y$.

Therefore, we attempt to ensure Def. 2 through a particularly small L_∞ -constraint on the perturbation, specifically $\|\zeta\|_\infty \leq \eta$ with $\eta = 0.1$ where ζ is the perturbation applied in the latent space. Still, as can be seen in Fig. 16, on-manifold adversarial examples might cross class boundaries, i.e., they change their actual label rendering them invalid according to our definition.

In Fig. 17, we clearly distinguish between on-class-manifold and on-data-manifold adversarial training, corresponding to the used class-specific or -agnostic VAE-GANs. Robustness, however, is measured wrt. on-data-manifold adversarial examples. As can be seen, the positive effect of on-manifold adversarial training diminishes when using on-data-manifold adversarial examples during training. Both, on FONTS and EMNIST, generalization slightly decreases in comparison to normal training because adversarial examples are not useful for learning the task if label invariance cannot be ensured. When evaluating robustness against on-data-manifold adversarial examples, however, the relation of on-data-manifold robustness to generalization can clearly be seen. Overall, this shows that this

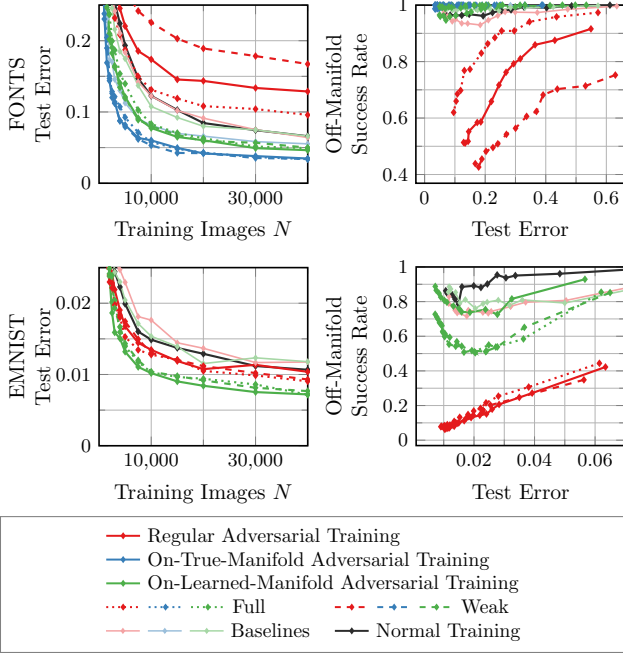


Figure 18: Adversarial training variants and baselines on FONTS and EMNIST. For adversarial training, we consider the *full variant*, i.e., training on 100% adversarial examples, and the *weak variant*, i.e., stopping the inner optimization problem of Eq. (17) as soon as the first adversarial example is found. For regular adversarial training, the strength of the adversary determines the robustness-generalization trade-off; for on-manifold adversarial training, the ideal strength depends on the approximation quality of the used VAE-GANs.

relationship also extends to more general, less strict definitions of on-manifold adversarial examples.

H. Baselines and Adversarial Training Variants

In the main paper, see Section 3.1, we consider the adversarial training variant by Madry et al. [62], i.e.,

$$\min_w \sum_{n=1}^N \max_{\|\delta\|_\infty \leq \epsilon} \mathcal{L}(f(x_n + \delta; w), y_n), \quad (17)$$

where f is the classifier with weights w , \mathcal{L} is the cross-entropy loss and x_n, y_n are training images and labels. In contrast to [62], we train on 50% clean and 50% adversarial examples [92, 30]. The inner optimization problem is run for full 40 iterations, as described in Section E without early stopping. Here, we additionally consider the *full variant*, i.e., training on 100% adversarial examples; and the *weak variant*, i.e., stopping the inner optimization problem as soon as the label changes. Additionally, we consider random perturbations as baseline, i.e., choosing the perturbations δ uniformly at random without any optimization. The

same variants and baselines apply to on-manifold adversarial training and adversarial transformation training.

In Section 3.6 of the main paper, we observed that different training strategies might exhibit different robustness-generalization characteristics. For example, regular adversarial training renders the learning problem harder: in addition to the actual task, the network has to learn (seemingly) random but adversarial noise directions leaving the manifold. In Fig. 18, we first show that training on randomly perturbed examples (instead of adversarially perturbed ones) is not effective, neither in image space nor in latent space. This result highlights the difference between random and adversarial noise, as also discussed in [23]. For regular adversarial training, the strength of the adversary primarily influences the robustness-generalization trade-off; for example, the weak variant increases generalization while reducing robustness. Note that this effect also depends on the difficulty of the task, e.g., FONTS is considerably more difficult than EMNIST. For on-manifold adversarial training, in contrast, the different variants have very little effect; generalization is influenced only slightly, while regular robustness is – as expected – not influenced.

I. Definition of Adversarial Examples

Adversarial examples are assumed to be label-invariant, i.e., the actual, true label does not change. For images, this is usually enforced using a norm-constraint on the perturbation – e.g., cf. Eq. (12); on other modalities, however, this norm-constraint might not be sufficient. In Section 3.3 of the main paper, we provide a definition for on-manifold adversarial examples based on the true, underlying data distribution – as restated in Def. 2. Here, we use this definition to first discuss a simple and intuitive example before considering the theoretical argument of [97], claiming that robust and accurate models are not possible on specific datasets; an argument in contradiction to our results

Let the observations x and labels y be drawn from a data distribution p , i.e., $x, y \sim p(x, y)$. Then, given a classifier f we define adversarial examples as follows:

Definition 3 (Adversarial Example). Given the data distribution p , an adversarial example for x with label y is a perturbed version \tilde{x} such that $f(\tilde{x}) \neq y$ but $p(y|\tilde{x}) > p(y'|\tilde{x}) \forall y' \neq y$.

In words, adversarial examples must not change the actual, true label wrt. the data distribution. Note that this definition is identical to Def. 2 for on-manifold adversarial examples. For the following toy examples, however, the data distribution has non-zero probability on the whole domain or we only consider adversarial examples \tilde{x} with $p(\tilde{x}) > 0$ such that Def. 3 is well-defined. We leave a more general definition of adversarial examples for future work.

We illustrate Def. 3 on an intuitive, binary classification

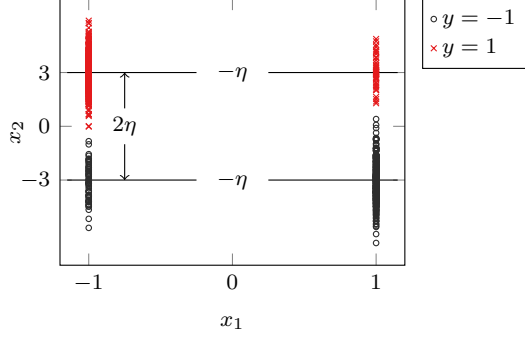


Figure 19: Illustration of the toy dataset considered by Tsipras et al. in [97] and defined in Eq. (21). For labels $y = 1$ and $y = -1$, the two-dimensional observations $x \in \{-1, 1\} \times \mathbb{R}$ are plotted. The first dimension, i.e., x_1 , mirrors the label with probability 0.9; the second dimension, i.e., x_2 , is drawn from a Gaussian $\mathcal{N}(y3, I)$, i.e., η from the text is 3. As illustrated on the left, perturbing an observation x with label $y = 1$ but $x_1 = -1$ by $2\eta = 6$ results in an adversarial example \tilde{x} indistinguishable from observations with label $y = -1$.

task. Specifically, the classes $y = 1$ and $y = -1$ are uniformly distributed, i.e., $p(y = 1) = p(y = -1) = 0.5$ and observations are drawn from point masses on 0 and ϵ :

$$p(x = 0|y = 1) = 1 \quad (18)$$

$$p(x = \epsilon|y = -1) = 1 \quad (19)$$

This problem is linearly separable for any $\epsilon > 0$; however, it seems that no classifier will be adversarially robust against perturbations of absolute value ϵ . For simplicity, we consider the observation $x = 0$ with $y = 1$ and the adversarial example $\tilde{x} = x + \epsilon = \epsilon$. Then, verifying Def. 3 yields a contradiction:

$$0 = p(y = 1|x = \epsilon) \not\approx p(y = -1|x = \epsilon) = 1. \quad (20)$$

It turns out, $\tilde{x} = \epsilon$ is not a proper adversarial example. This example illustrates that an exact definition of adversarial examples, e.g., Def. 3, is essential to study the robustness of such toy datasets.

I.1. Discussion of [97]

In [97], Tsipras et al. argue that there exists an inherent trade-off between regular robustness and generalization based on a slightly more complex toy example; we follow the notation in [97]. Specifically, for labels $y = 1$ and $y = -1$ with $p(y = 1) = p(y = -1) = 0.5$, the observations $x \in \{-1, 1\} \times \mathbb{R}$ are drawn as follows³:

³Note that, for simplicity and convenience, we consider the 2-dimensional case; Tsipras et al. consider the general D -dimensional case, where x_1 remains unchanged and x_2, \dots, x_D are drawn from the corresponding Gaussian, cf. (21).

$$p(x_1|y) = \begin{cases} p & \text{if } x_1 = y \\ 1 - p & \text{if } x_1 = -y \end{cases}, \quad (21)$$

$$p(x_2|y) = \mathcal{N}(x_2; y\eta, 1)$$

where η defines the degree of overlapping between the two classes and $p \geq 0.5$. Fig. 19 illustrates this dataset for $p = 0.9$ and $\eta = 3$. For a L_∞ -bounded adversary with $\epsilon \geq 2\eta$, Tsipras et al. show that no model can be both accurate and robust. Specifically, for x with $y = 1$ but $x_1 = -1$ and $x_2 = \eta$, we consider replacing x_2 with $\tilde{x}_2 = x_2 - 2\eta = -\eta$, as considered in [97]. However, this adversary does not produce proper adversarial examples according to our definition. Indeed,

$$\begin{aligned} p(y = 1|x = \tilde{x}) &= p(y = 1|x_1 = -1) \cdot p(y = 1|x_2 = -\eta) \\ &= (1 - p) \cdot \mathcal{N}(x_2 = -\eta; \eta, 1) \\ &\not\approx p \cdot \mathcal{N}(x_2 = -\eta; -\eta, 1) \\ &= p(y = -1|x_1 = -1) \cdot p(y = -1|x_2 = -\eta) \\ &= p(y = -1|x = \tilde{x}) \end{aligned} \quad (22)$$

which contradicts our definition. Thus, in light of Def. 3, the suggested trade-off of Tsipras et al. is questionable. However, we note that this argument explicitly depends on our definition of proper and invalid adversarial examples, i.e., Def. 3; other definitions of adversarial examples or adversarial robustness, e.g., in the context of the adversarial loss defined in [97], may lead to different conclusions.

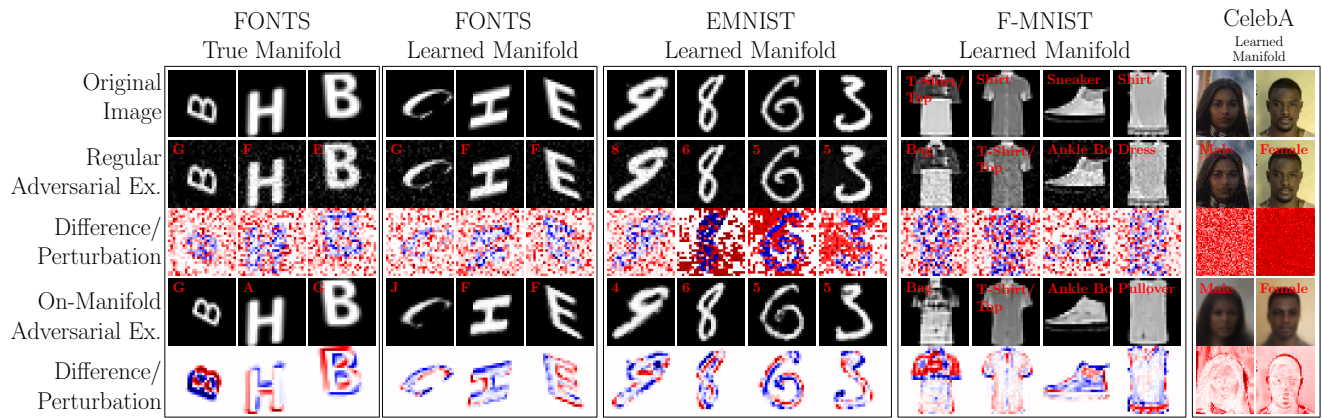


Figure 20: Regular and on-manifold adversarial examples on FONTS, EMNIST, F-MNIST and CelebA. On FONTS, the manifold is known; otherwise, class manifolds have been approximated using VAE-GANs. In addition to the original test images, we also show the adversarial examples and their (normalized) difference (or the magnitude thereof for CelebA).